Title:

Impaired Epigenesis of Imprinting Predispositions Causes Autism-like Behavioral Phenotypes in Domestic Chicks

Authors:

Toshiya Matsushima[1,5]*, Momoko Miura[1], Nina Patzke[1,2], Noriyuki Toji[1], Kazuhiro Wada[1], Yukiko Ogura[3], Koichi J. Homma[4], Paola Sgadò[5], Giorgio Vallortigara[5]

Affiliations:

1: Department of Biology, Faculty of Science, Hokkaido University, Sapporo, Japan

2: Health and Medical University, Potsdam, Germany

3: Information Science and Technology, University of Tokyo, Tokyo, Japan

4: Department of Molecular Biology, Faculty of Pharmaceutical Sciences, Teikyo University, Tokyo, Japan

5: Center for Mind/Brain Science, University of Trento, Rovereto, Italy

*: corresponding author

e-mail: matsushimatoshiya@gmail.com

Graphical summary

Highlights

- Imprinting of artifact canalizes predisposed preference to biological motion (BM).
- Fetal VPA injection impairs imprinting and spares BM preference in hatchlings.
- Blockade of nAChR by ketamine or imidacloprid spares imprinting and impairs BM.
- Underlying molecular actions are dissociated between the two sets of chemicals.
- However, VPA and nAChR blockade impaired the imprinting of biological images.
- Both impairments are rescued by postnatal bumetanide.

Abstract

Several environmental chemicals are suspected as risk factors for autism spectrum disorder (ASD), including valproic acid (VPA) and pesticides acting on nicotinic acetylcholine receptor (nAChR) if exposed during pregnancy. However, their target processes in fetal neuro-development are unspecified. We report that VPA effectively suppressed the spontaneous motion of 14-day fetuses, and selectively impaired the imprinting of an artifact object (colored toy) in hatchlings while the predisposed preference to biological motion (BM) remained intact. However, blockade of nAChR (by ketamine, tubocurarine, and imidacloprid, a neonicotinoid insecticide) similarly suppressed the fetal motion, but spared imprinting and impaired BM. The underlying molecular and cellular actions were dissociated between the two sets of chemicals. When hatchlings were trained using merged two point-light animations in different colors, VPA and ketamine similarly inhibited the formation of selective preference for the biological image, indicating common hypoplasia in social attachment formation. Fetal epigenesis of BM predisposition and imprinting memory is critical for adaptive socialization of neonates.

Introduction

Despite heterogeneous diagnostic phenotypes and genetic backgrounds, autism spectrum disorder (ASD) is primarily characterized by impaired social interactions[1,2]. Visual predisposition to animate objects typically arises early in life[3-6], which is hampered in neonates/juveniles with ASD or its familial risk[7-14]. Along with genetic factors, exposure to environmental chemical agents, such as anticonvulsant drugs (valproic acid VPA[15-18]) and environmental pollutants including endocrine disruptors and pesticides during pregnancy could be an ASD risk factor [19-25]. Despite intensive efforts to develop mammalian models to assess these genetic and environmental factors that act on epigenetic processes of neuro-development[26-28], the validity is limited because these neonatal mammals (mostly, rodents) do not autonomously perceive biological motion (BM) in early life, which is found only in human neonates[3-5] and a taxonomically distant animal, domestic chicks[29,30].

The ability to visually perceive conspecifics, as well as identify individuals, their emotions and intention by highly reduced stimuli (such as point light animations) is

referred to as the BM perception[31]. Generally, motion perception develops slowly in human neonates with early visual experiences exerting significant influences[32]. Pre-attentive processing of biologically relevant stimuli (such as BM and face configuration) is assumed to canalize the subsequent memorization, leading to the adaptive formation of social attachment to specific individuals[4]. Human neonates typically show an early emergence of BM preference[3,5,6], which most non-human animal species do not reveal except newly-hatched domestic chicks[29,30]. Various non-human animals (zebrafish[33], pigeons[34], cats[35], rats[36], baboons[37] and chimpanzees[38]) discriminate BM point-light animations, but only after intensive rewarded training trials; these animals do not spontaneously show BM preference just after birth.

Similar to human neonates, visually naïve chicks show a BM preference[29,30] that is further enhanced by imprinting of an artifact (non-BM) object[39], facilitating and canalizing the subsequent imprinting[40,41]. Along with the commonality in the early development of BM, humans and chicks show inversion effects, namely predisposition to up-right walking configuration (humans[42,43], chicks[30]). Assuming a significant difference in the brain organization between these two species[44,45], the functional and developmental similarities are striking. Although the neural substrates of the neonatal BM perception are largely unspecified[46], recent studies on the sub-cortical visual processing suggest the involvement of evolutionarily conserved visual systems[47-49], i.e., early visual pathways through superior colliculus (or optic tectum in birds) and pulvinar (or nucles rotundus) are critical[50-51]. Pioneering studies revealed the effects of fetal VPA application on social behaviors[52-54] but the BM preference has not been addressed.

A question arises regarding this context. What prenatal processes construct the BM preference? Specifically, if the VPA effect on behavioral hypoplasia was mediated by well-documented action as an inhibitor of histone deacetylation[55], what other risk agents were used? As VPA is a potent anti-convulsant drug, it might effectively suppress the fetal motions, hence, the BM preference. We hypothesized that suppression of spontaneous fetal motions[56-58] is responsible, where excitatory GABA actions could play a role[59-61]. In human adults, execution of an unfamiliar motor patterns facilitates perception of the corresponding BM animations, thus, non-visual motor execution might be involved[62]. According to the motor involvement, an imaging study suggested

contribution of the posterior part of cerebellum in BM perception63. If this applies to fetuses, any chemical agents that suppress spontaneous motion, including the blockade of neuro-muscular transmission, would impair the development of BM preference. As the first step, we listed agents that effectively suppress the fetal motion at embryonic day 14 (E14), the stage wherein VPA is reported to be effective52-54.

Results

Recording the spontaneous fetal motion; ballistography

The spontaneous fetal motion was reliably detected by placing an analog record stylus against the shell surface (**experiment 1, Fig.1A**). Low frequency power (2~20 Hz) of the recorded signal (ballistogram64; see supplement 1.2.) revealed that VPA injection to the air sac acutely suppressed the motion (**B**). Similar suppression was found by ketamine (sedative drug of a wide action spectrum including blockade of NMDAR and nAChR), mk801 (selective NMDAR blocker), and tubocurarine (nAChR blocker of a wide spectrum) (**Fig.1C**; see supplement 1.5. and 2.1. for the chemical agents used and statistics). Among other nAChR blockers, methyllycaconitine citrate (MLA, specific to neuronal α7 subtype), and dihydro-β-erythroidine hydrobromide (DHβE, specific to muscular α4β2 subtype) were similarly effective. Superimposed traces of ballistography (**Fig.S1**) show transient suppression for ~90 min, whereas mk801 and DHβE caused more intensive suppression lasting for more than 3 hours. Suppression was dose-dependent in all tested agents (**Fig.S2A**). Fetal motion is sensitive to the blockade of cholinergic or NMDA-R mediated neurotransmission in the brain (VPA, ketamine, mk801, and MLA), and neuro-muscular junctions in the periphery (DHβE); tubocurarine can act centrally and peripherally.

BM preference and imprinting of hatchlings; behavioral pharmacology

Hatchlings from the injected eggs were tested for BM preference and imprinting (**experiment 2, Fig.1D**; supplement 1.3., 1.4., 2.2.). Chicks were individually trained by a video clip of a rotating red toy (displayed on an LCD with sound) for two hours with one hour intermission, and after 30 to 60 min, tested for BM preference (walking point-light animation over linear motion) and for imprinting memory (familiar red toy over novel yellow). Among the examined agents, ketamine, tubocurarine and MLA

significantly reduced BM preference compared with control in a dose-dependent manner, while VPA, mk801 and DHβE failed (**Figs.1Ea, S3C**). Significant reduction in the motor activities during training (total count of approach running) was not found except ketamine (**Fig.S4**). Despite effective suppression of the fetal motion, mk801 failed to cause any behavioral effects, and hence, VPA and ketamine should act through pathways other than NMDA-R. Moreover, nAChR is responsible for the BM preference impairment because ketamine, tubocurarine and MLA were similarly effective. Notably, besides NMDA-R suppression, ketamine directly blocks the nAChR-associated channels in the central nervous system and peripheral tissues65-68. When injected into E10 and E18, tubocurarine did not significantly impair BM (**Fig.S3B**) showing cholinergic transmission's critical role around E14. However, VPA spared BM and impaired imprinting (**Figs.1Eb, S3D**), indicating doubly dissociated pharmacology between these two behavioral traits, except that MLA and DHβE weakly suppressed imprinting. Suppression of fetal motion is not sufficient for the BM preference impairment in hatchlings.

Blockade of nAChR by imidacloprid (IMI) also impaired BM (**experiment 3, Fig.2B;** supplement 2.3.). When applied to E14, IMI suppressed fetal motion at the low dose (5μg/egg, **Fig.2A**), and significantly impaired BM but spared imprinting on hatchlings (**2Ba,b**). As a human fetus could be maternally exposed to ambient neonicotinoids, we tested the IMI effect injected into fertilized eggs before incubation (E0, **Fig.2B**). The treated hatchlings showed a dose-dependent significant impairment of BM at 50 μg/egg or lower. Plotting the imprinting score against the BM (**Fig.1Ec**) revealed that, regarding the aforementioned VPA case (**Fig.1Ec**), those with a low BM score showed a lower imprint score in groups that received a high dose of IMI (50 μg/egg, both E0 and E14). Further two-dimensional analysis of BM/imprint scores using Mahalanobis distance revealed effects of VPA, ketamine, MLA, and IMI (**Fig.S4**), although significance level was achieved only in VPA.

BM preference canalizes the subsequent imprinting40,41. If chicks were trained by a non-biological artifact (rotating toy in red) on the post-hatch one day (P1), they were oriented to a biological object (walking point in yellow, Wp[yellow]) on the subsequent day (P2; **experiment 4, Fig.3;** supplement 2.5.). Injection of ketamine and tubocurarine (but not VPA) on E14 suppressed BM preference on P1 (**Fig.3B**) as in **experiment 2**.

However, the second P2 training using merged point-light animations (linear motion in red and walking in yellow, Lp[red]+Wp[yellow]) resulted in the impaired formation of preference for Wp[yellow] in all groups (imprinting_1 score in **Fig.3Ca**), while preference to the artifact (red toy) remained intact except VPA (imprinting_2 score in **Da**). Multiple regression analysis of the imprinting_1 score revealed a significant interaction of BM score and the examined drugs (VPA, ketamine, and tubocurarine). The blockade of nAChR impairs the formation of social attachment similar to VPA through distinct processes.

Histone acetylation, brain weight and neuronal maturation; development

The nAChR blockers' effect should be distinct from VPA, that is shown to act as a potent inhibitor of histone deacetylases (HDACs)18. To confirm the VPA action, we examined histone acetylation in primary cell culture prepared from E14 embryonic telencephalon (**experiment 5, Fig.4A;** supplement 2.6.). As expected, VPA increased the H3K27 acetylation level at a dosage comparable to the *in ovo* injection (0.12~1.2 mM of medium), whereas ketamine had no effects at 6.6 and 66 µg/mL which is higher than the *in ovo* dose (0.2mg/50g = ca. 4 µg/mL).

Brain morphology could also differ in these chicks with different treatments. Although controversial, macrocephaly (increased head/brain size) is associated with some ASD subtypes due to altered neurogenesis in the early infantile period69-71. In chicks, the whole-brain weight of hatchlings revealed that E14 injection of VPA, but not ketamine, significantly decreased the brain weight (**experiment 6, Fig.4Ba;** supplement 2.7.) compared to control, without changes in the body weight (**Fig.S5**). Notably, ~21% (11 out of 53 chicks) had a distinctly small brain, whereas the rest remained in the control range. Male brains were significantly bigger, but no significant interaction occurred between sex and treatment. The total cell number estimated by isotropic fractionation (**Fig.4Bb**) failed to show a difference by treatment, but a significantly lower ratio of NeuN-positive cells occurred in VPA (**Bc**). Perturbation of gene expression by VPA could lead to retardation of brain development during the late pre-hatch stage and, hence, the delayed maturation of neurons.

Composition of nAChR subunits and GABA switch; gene expression

We also examined the physiological aspects of brain development. As nAChR could play a critical role in the late phase of fetal development, we focused on subunits (*α4* and *α7*) in three brain regions critically involved in imprinting and visuo-motor coordination72-74; IMM (intermediate medial mesopallium for imprinting), arco (arcopallium for limbic and motor functions) and tectum (optic tectum for visuo-motor coordination) at three developmental stages (E14, E18, and P1) (**experiment 7**). qPCR analysis (supplement 1.8., 2.8.) revealed a distinct regional difference in the *α4*/*α7* ratio, but not in the stages (**Fig.4Ca**). Specifically, *α4* was dominant in IMM, intermediate in arco, and *α7* was dominant in tectum throughout the stages.

Neuronal maturation is accompanied by a decrease in the intracellular Cl^-, thus there is a switch from excitation to inhibition by GABA-A transmission59-61. This change referred to as GABA switch, is caused by $[Cl^-]_i$ decrease through increased activity of K-Cl cotransporter 2 (KCC2) compared to Na-K-Cl cotransporter 1 (NKCC1). As shown in **Fig.4Cb**, the ratio of the corresponding genes (*slc12a2* for NKCC1 vs. *slc12a5* for KCC2) revealed a significant decrease in regional differences and significant decrease in IMM and arco but small in the tectum. This pattern paralleled the increase in NeuN gene expression (*sbfox3* normalized by *GAPDH*) in all three tested regions (**Cc**) with significant negative correlations (**Cd**).

VPA caused a marginally significant increase in the *slc12a5/slc12a2* ratio (suggesting a delayed GABA switch) selectively in the tectum (**Fig.4Ce**). Multiple regression analysis revealed p=0.067 for the significance of the interaction term of tectum*VPA (n=6), whereas no such effects occurred in other interactions and the tubocurarine group (**Cf**, supplement 2.8.). There were no significant differences in the *α4*/*α7* ratio or *sbfox3* expression in VPA and tubocurarine. Thus, we predicted that pharmacological blockade of NKCC1 by bumetanide could rescue the impairment effects of VPA. Inconsistently to the isotropic fractionation data of the whole telencephalon (**Fig.4Bc**), VPA failed to reduce the *sbfox3* expression IMM and arco (**Fig.S9B**); we must be cautious of the NeuN.

Bumetanide rescued the impairment by VPA and tubocurarine; behavioral pharmacology

First, we tested if bumetanide (NKCC1 blocker) and VU0463271 (KCC2 blocker)

suppress the spontaneous fetal motion at E14 but there were no significant effects (**Fig.5A**, supplement 2.9.). However, the chicks that received an E14 injection of bumetanide or VU0463271 of the same doses showed a significantly impaired BM preference while imprinting remained intact (**Fig.S3C, D**). Therefore, suppression of fetal motion is not necessary for BM impairment. When applied to P1 chicks before training (30 min before the start of the training session), bumetanide rescued behavioral impairments by VPA and tubocurarine, imprinting for VPA and BM for tubocurarine (**Fig.5Ba,b, Fig.S10**).

BM preference and imprinting memory contribute to the successful formation of social attachment to biological objects through distinct neuro-developmental mechanisms through heterogenous pathogeneses. Pharmacological inhibition of fetal motion is not necessary or sufficient for suppressing the development of behavioral socialization processes in hatchlings. Delayed development of the early sub-cortical (sub-pallial) visual pathways could cause social hypoplasia in hatchlings and human

Discussions

Plausible scenario of the adaptive socialization through imprinting

Since Lorenz75, imprinting has been assumed as a simple but unusual type of learning in limited precocial animals, where irreversible one-time learning occurs in a restricted short critical period after birth. This study series suggest a different figure: imprinting is composed of multiple processes and mechanisms functioning together (see **graphical summary**). In the early neonatal processes, exposure to any moving object leads to the CONCPEC mechanism76 associated with the thyroid hormone (specifically, triiodo-thyronine T_3) influx, which is induced by imprinting and, in turn, elongates the sensitive period77-79 and enhances innate predispositions80-82. Therefore, subsequent secondary imprinting is canalized to objects bearing biological features, namely, the CONLERN mechanism is activated toward adaptive social attachment. These early processes, which are quite homologous to that proposed for neonatal development in humans48,83, are based on epigenetic processes of neuro-development in the fetus. This report shows two distinct aspects of these processes, one impaired by VPA and another by the nAChR blockers. Impairment in either the memory formation (by VPA) or the BM predisposition (by nAChR blockers) leads to a common disorder characterized as

social attachment hypoplasia. However, details of the pathogenesis are unspecified.

Optic tectum is a possible target of the VPA action and the amendment by bumetanide

Contrary to our initial expectation, this qPCR study suggested that VPA causes a delayed GABA switch in the optic tectum, but not in IMM and arco that are critical for imprinting[73,74]. As the avian homolog of the mammalian superior colliculus (SC), the tectum is the major subpallial (subcortical) center of multimodal visuo-auditory integration and motor coordination[84-87]. Recent studies have shown that SC has orientation columns[88] and contributes to social interaction[89], thus its signal processing could be almost on par with those in the visual cortices. Even after the correspondence between ASD and the integrative nature of SC was theoretically argued for[51,90], the link has not been experimentally addressed.

To examine this linkage, it is important to ask if tectum/SC is the target of the systemic bumetanide treatment. Although the recent phase-2 trial had a negative outcome[91], bumetanide is considered a valid candidate therapeutic agent for ASD, as it effectively facilitates the maturation of GABAergic inhibition[92,93]. In concert, the sensitive period of filial imprinting is also sensitive to the GABA-A receptor manipulation[94], as of the experience-dependent reorganization of the primary visual cortex in mammals[95,96]. A further extensive survey is needed to identify the brain regions responsible for the GABA-dependent control of the sensitive period of imprinting.

Possible central and peripheral targets of the nAChR blockade

Nicotinic transmission is critical for neurodevelopment[97-99] including the pathophysiology of ASD[100-102]. However, as nAChR is widespread in the brain and body[103-105], several brain regions/organs must be considered. Among the possible candidates, the following regions need specific attention: (1) cholinergic neurons in the striatum and the basal forebrain projecting to wide areas in pallium (or cortex in mammals)[106], (2) cholinergic neurons in nucleus isthmi parvocellularis (or pedunculo-pontine tegmental nucleus) projecting to optic tectum (superior colliculus)[107-109], and (3) pre-ganglionic cholinergic terminals of parasympathetic nerve acting on thyroid gland[110]. If (1) is the case, involvement of telencephalon in the BM predisposition

should be considered as delayed GABA switch may be an underlying factor in the brain areas along with IMM, arco and tectum. If (2), retarded visual attention due to the underdeveloped tecto-isthmo-tectal network must be considered. If (3), hypothyroidism during gestation or early neonatal period could be the target as reported in human neonates111-113 and chicks77,80. The responsible regions' specification will enable us to design appropriate amendments for each phenotype.

Neonicotinoids as an environmental risk factor for ASD

Environmental risk of neonicotinoids was initially related to the population decline of insectivorous birds114 and the delayed migration by impaired foraging behavior115,116. Recently, the association between ambient neonicotinoids and ASD in humans has been identified in several extensive epidemiological studies117-120. Fetal/neonatal exposure of acetamiprid neonicotinoid caused abnormal development of socio-sexual behavior in mice121. Despite the low level of acute toxicity, low affinity for vertebrate nAChR, and rapid metabolism122, neonicotinoids are known for a high persistence level. As shown in this study, identical effective dosage occurred between E0 and E14 groups (experiment_3), indicating a strong residual effect. IMI suppressed BM preference nearly completely at 1ppm (50μg / 50g egg), which was significantly lower than the lethal level (31-50 mg/kg BW in quails, pigeons, and sparrows)122. Legislation on the control of residual neonicotinoids and other pesticidal chemicals in feed, meat, and eggs should consider the risk of increase in the ASD cases by nicotinic blockers.

Advantages and limitations of chicks for screening of ASD risk agents

This study suggests that the domestic chick is a valid animal model123,124 for studying ASD, even though birds are taxonomically distant from humans. (1) Chick has construct validity because there are common causes and processes, such as VPA, blockade of nAChR, and involvement of GABA transmission and delayed GABA switch. (2) Chick uniquely has face validity because BM preference and learned social attachment formation are assayed. (3) Chick could also have predictive validity because bumetanide rescued the learning impairment by VPA and tubocurarine. We must also consider the recent development of a rich repertoire of behavioral paradigms available

in domestic chicks125-130, ranging from spatial representation, numerical comprehension, and arithmetic to the social rank and link to cognitive capability. ASD is characterized by the impaired social interactions and other symptoms such as delayed speech, learning disability, repetitive stereotyped behaviors, and altered (reduced or sensitized) sensory perception, which we may address using chicks as the model, including a longitudinal life-long survey of these treated chicks.

Although inferior in the homological validity124, the chick model has several advantages over conventional mammalian model animals. (1) Maternal complication is disregarded, whereas gestational effects are inevitably subjected to the maternal metabolism in mammals. The time course and effective dose of agents are precisely determined. (2) The short incubation period facilitates speedy screening, as it takes only a week from the injection of chemicals to E14 eggs until the hatchling are tested on P1. (3) Simple imprinting paradigm allows testing of predisposed preference and learning ability. Humans are often exposed to several ASD risk factors simultaneously, so the link between the predispositions and the learned phenotypes is often confounded. The chick model is suitable for examining interactions of these agents in a strictly controlled manner by monitoring heterogeneous aspects of the disabilities.

A major limitation of the chick model is the difficulties in genetic controls. Despite domesticated, inbred strains are yet not available in birds because of the severe inbreeding depression131. Interactions between genetic factors and the ambient risk agents are rarely studied without the development of genetically controlled/manipulated chickens. The introduction of genetic engineering is expected.

Figure legends

Figure 1.

Spontaneous fetal motion and development of biological motion (BM) preference in the hatchlings. **(A, B)** Ballistography recording (experiment 1) and blockade by sodium valproate (VPA). Record stylus placed against the eggshell surface detected the miniature vibration caused by spontaneous fetal motion. **(C)** The dose was experimentally searched for each agent so that fetal motion was similarly suppressed on embryonic day 14 (E14), while hatchlings were normally trained. **(D)** Training and test procedures (experiment 2). Chicks were trained by an artifact object (rotating red toy)

accompanied by synchronous sound and tested by binary choices for BM and imprinting; stay time difference (sec) was used for the score. **(E)** BM score (**a**) and imprinting score (**b**) of the treated hatchlings were plotted (**c**). Number in parenthesis indicates the sample size; control data included batch-matched data for all experiments (see supplementary **Figure S3**). Asterisks indicate the significant difference from the control by multiple regression analysis; *, $p<0.05$, **, $p<0.01$, ***, $p<0.001$ in figures.

Figure 2.

Imidacloprid (IMI) suppressed the fetal motion on E14 and blocked BM preference and imprinting of hatchlings (experiment 3). (**A**) Effects of 5~50μg/egg (0.1~1ppm) were compared with the control (same dataset in Figure 1C). (**B**) IMI injection on E0 and E14 similarly impaired BM (**Ba**) and imprinting (**Bb**); **Bc** shows the plot. Control data of batch-matched (identical genetic backgrounds, n=71) were included.

Figure 3.

The two-step imprinting paradigm revealed common hypoplasia by E14 injection of VPA and nAChR blockade (experiment 4). (**A**) Behavioral procedure. After the post-hatch 1-day (P1) training using an artifact (rotating red toy) and BM test, chicks received the second day (P2) training, wherein two images of point light animations were presented with yellow in walking (Wp[yellow]) and red in linear rigid motion (Lp[red]). (**B**) BM scores confirmed. (**Ca,b**) Both VPA and ketamine chicks showed the impaired formation of preference to Wp[yellow]. Notably, the tubocurarine chicks showed similar plots to the ketamine, whereas the imprinting score of the VPA was no more dependent on the BM score (**Cb**). (**Da,b**) VPA chicks showed the impaired imprinting to artifact red toy as in experiment 3. Notably individuals with high BM scores showed normal imprinting_2 scores.

Figure 4.

Distinct effects of VPA and nAChR blockade on histone acetylation, brain size and neuron number, and gene expression profiles. (**A**) VPA but not ketamine enhanced the acetylation level of histone H3K27 in primary cell culture made from E14 telencephalon. (**B**) VPA but not ketamine reduced the brain weight (**Ba**), and the ratio of

NeuN positive cells measured by isotropic fractionation (**Bc**); total cell number was not affected (**Bb**). Male brains were significantly heavier, but no interaction was found between the sex and the agents. No significant effects of sex were detected on the cell number and the NeuN ratio. (**C**) Subunits of nAChR (*α4*/*α7* ratio; **Ca**), cation-linked chloride cotransporters (*slc12a2* for NKCC1, *slc12a5* for KCC2; **Cb**), and NeuN (*sbfox3* normalized by *GAPDH*; **Cc**) were compared at three stages (E14, E18 and P1) in three brain regions (IMM, arcopallium and optic tectum). IMM served as the reference for the regional comparisons, and E14 for the developmental stages. The ratio of cotransporters and the NeuN showed a significantly negative correlation along with development in all brain regions (**Cd**). The ratio of chloride cotransporters was examined in VPA (**Ce**) and tubocurarine chicks (**Cf**). Marginally significant interaction (p=0.067) was found in the tectum of VPA chicks, whereas not significant in others.

Figure 5

Bumetanide rescued the behavioral effects of VPA and nAChR blockade. Bumetanide (and VU0463271 as well) failed to suppress the fetal motion on E14 (**A**). When applied in hatchling, bumetanide effectively rescued the impaired BM score by ketamine / tubocurarine (**Ba**) and the imprinting impairment by VPA (**Bb**). The bumetanide data were compared with those obtained in experiment_2 (indicated by #, Figure 1Ea,b).

Figure S1.

The results of preliminary experiment_0. Four groups of eggs received an injection of VPA on E14, and the hatchlings (n=10 or 11) were trained either by a red toy (**Aa**) or a yellow toy (**Ab**), then tested for BM preference and the imprinting memory in the same manner. Behavioral tests revealed similar results, with the red toy data but more evident than the yellow (**Ba,b,c**). ANOVA statistics revealed significant effects of drug and color in the imprinting score (**C**). The red toy data were included in experiment_2.

Figure S2.

Superimposed ballistographies recorded in experiment_1; n denotes the number of eggs. Control eggs received injection of 200μL distilled water. The power of the ballistogram was averaged at every min and plotted against time (0 to 120 min) with the injection

time set at 30 min (vertical dashed lines). The weight of chemicals shown in parenthesis was injected per egg, which weighed ~50g excluding the eggshell on E14.

Figure S3.

Details of the experiment_1 and 2 data. (**A**) Ballistography index of the post-injection 90 min data normalized by the pre-injection 30 min record. (**B**) Imprinting score plotted against BM score in the groups shown in **Figure 1Ec**. (**C,D**) BM and imprinting scores compared with the control data at the left end. All of the accepted data from experiment_2, 3, and 8 were included.

Figure S4.

The run number during the training (run) were compared among the experiment_1 and 2 data. (**A**) Significantly lower run appeared only in the ketamine (0.20mg) group (* $p<0.05$). (**B**) No significant correlations occurred between the run and the imprinting scores.

Figure S5.

Mahalanobis distance (MD) analysis of experiments_2 and 3 data; supplementary materials 2.4. Each group of experimental chicks was represented by the gravity center (mean values) of BM and imprinting scores as (x, y), and the distance of the group was determined from the gravity center of the control dataset. Considering the weak but significant correlation between the two scores in the control ($r=0.21$, $p<0.05$), the Euclidian distance was adjusted according to the method by Taguchi & Rajesh (2000). (**A**) Ten individuals were randomly sampled from the control dataset (n=123) repetitively 10,000 times, and the MD distance of each sample was measured. The calculated distance (10,000 samples) was converted to the probability density. Levels at 90%, 95%, 99%, and 99.9% are indicated by vertical lines. (**B**) MD distance of experimental groups from the control dataset was calculated after normalization by the sample size. Significantly large distances appeared only in the VPA group, and considerably large (but not significant) distances in ketamine, MLA, and IMI groups.

Figure S6.

The body weight of the chicks examined in experiment_6. No significant differences were found among groups and between sexes.

Figures S7-9.

Details of qPCR measurement of gene expressions in Experiment_7. Developmental changes (A), VPA (B) and tubocurarine (C) effects were plotted for the nAChR subtypes (*α4*, *α7*, and the ratio; **S7**), the chloride cotransporters (*slc12a2* (NKCC1), *slc12a5* (KCC2), and the ratio; **S8**), and the NeuN signal (*sbfox3* normalized by *GAPDH*, **S9**).

Figure S10.

Correlations between the imprinting score (y-axis) and the BM score (x-axis) were compared among groups with bumetanide treatment (experiment_8) and those without it (experiment_2).

Reference list

Main text

1. Wing L, Gould J. (1979). Severe impairments of social interaction and associated abnormalities in children: epidemiology and classification. *Journal of Autism and Developmental Disorders* 9: 11-29 (https://doi.org/10.1007/BF01531288)
2. American Psychiatric Association. Diagnostic and Statistical Manual of Mental Disorders. 5th ed. Washington: *American Psychiatric Association*; 2013.
3. Simion F, Regolin L, Bulf H. (2008). A predisposition for biological motion in the newborn baby. *Proceedings of the National Academy of Sciences* 105: 809-813 (https://doi.org/10.1073/pnas.0707021105)
4. Bardi L, Regolin L, Simion F. (2011). Biological motion preference in humans at birth: role of dynamic and configural properties. *Developmental Science* 14: 353-359 (https://doi.org/10.1111/j.1467-7687.2010.00985.x)
5. Sifre R, Olson L, Gillespie S, Klin A, Jones W, Shultz S. (2018). A longitudinal investigation of preferential attention to biological motion in 2- and 24-month-old infants. *Scientific Reports* 8: 2527 (https://doi.org/10.1038/s41598-018-20808-0)
6. Di Giorgio E, Lunghi M, Vallortigara G, Simion F. (2021). Newborns' sensitivity to speed changes as a building block for animacy perception. *Scientific Reports* 11: 542 (https://doi.org/10.1038/s41598-020-79451-3)
7. Rutherford MD, Pennington BF, Rogers SJ. (2006). The perception of animacy in young children with autism. Journal of Autism and Developmental Disorders 36: 983–992 (https://doi.org/10.1007/s10803-006-0136-8)
8. Klin A, Lin DJ, Gorrindo P, Ramsay G, Jones W. (2009). Two-year-olds with autism orient to non-social contingencies rather than biological motion. *Nature* 459: 257–261 (https://doi.org/10.1038/nature07868)
9. Di Gioggio E, Frasnelli E, Rosa-Salva O, Scattoni ML, Puopolo M, Tosoni D, NIDA-Network, Simion F, Vallortigara G. Difference in visual social predispositions between newborns at low- and high-risk for autism. (2016). *Scientific Reports* 6: 26395 (https://doi.org/10.1038/srep26395)
10. Wang Y, Wang L, Xu Q, Liu D, Chen L, Troje NF, He S, Jiang Y. (2018) Heritable aspects of biological motion perception and its covariation with autistic traits. *Proceedings of the National Academy of Sciences* 115: 1937-1942 (https://doi.org/10.1073/pnas.1714655115).
11. Todorova GK, Hatton REM, Pollick FE. (2019). Biological motion perception in autism spectrum disorder: a meta-analysis. *Molecular Autism* 10:49. (https://doi.org/10.1186/s13229-019-0299-8)
12. Fujioka T, Tsuchiya KJ, Saito M, Hirano Y. et al. (2020) Developmental changes in attention to social information from childhood to adolescence in autism spectrum disorders: a comparative study. *Molecular Autism* 11:24. (https://doi.org/10.1186/s13229-020-00321-w)
13. Federici A, Parma V, Vicovaro M, Radassao L, Casartelli L, Ronconi L. (2020). Anomalous perception of biological motion in autism: a conceptual review and meta-analysis. *Scientific Reports* 10:4576 (https://doi.org/10.1038/s41598-020-61252-3)
14. Kaliukhovich D, Manyakov NV, Bangerter A, Ness S, Skalkin A et al. (2021).

Visual preference for biological motion in children and adults with autism spectrum disorder: an eye-tracking study. *Journal of Autism and Developmental Disorders* 51:2369–2380 (https://doi.org/10.1007/s10803-020-04707-w)

15. Moore SJ, Turnpenny P, Quinn A, Glover S, Lloyd DJ, Montgomery T, Dean JCS. (2000). A clinical study of 57 children with fetal anticonvulsive syndromes. *Journal of Medical Genetics* 37: 489-497 (https://doi.org/10.1136/jmg.37.7.489)
16. Rasalam AD, Hailey H, Williams JHG, Moore SJ, Turnpenny PD, Lloyd DJ, Bean JCS. Characteristics of fetal anticonvulsant syndrome associated autistic disorder. *Developmental Medicine & Clinical Neurology* 47: 551-555 (https://doi.org/10.1017/S0012162205001076)
17. Bromley RL, Mawer GE, Briggs M, Cheyne C, Clayton-Smith J et al. (2013). The prevalence of neurodevelopmental disorders in children prenatally exposed to antiepileptic drugs. *Journal of Neurology, Neurosurgery & Psychiatry* 84: 637-643 (https://doi.org/10.1136/jnnp-2012-304270)
18. Christensen J, Grønborg TK, Sørensen MJ, Schendel D, Parner ET, Pedersen LH Vestergaard M. (2013) Prenatal valproate exposure and risk of autism spectrum disorders and childhood autism. *Journal of the American Medical Association* 309: 1696-1703 (https://doi.org/10.1001/jama.2013.2270)
19. Grandjean P, Landrigan PJ. (2014). Neurobehavioural effects of developmental toxicity. *Lancet Neurology* 13:330-338 (http://dx.doi.org/10.1016/S1474-4422(13)70278-3)
20. Lyall Schmidt RJ, Hertz-Picciotto I. (2014). Maternal lifestyle and environmental risk factors for autism spectrum disorders. *International Journal of Epidemiology* 43: 443-464 (https://doi.org/10.1093/ije/dyt282)
21. Keil AP, Daniels JL, Hertz-Picciotto I. (2014) Autism spectrum disorder, flea and tick medication, and adjustments for exposure misclassification: the CHARGE (Childhood Autism Risks from Genetics and Envinronment) case-control study. *Environmental Health* 13:3 (https://doi.org/10.1186/1476-069X-13-3)
22. GunierRB, Bradman A, Harley KG, Kogut K, Eskenazi B. (2017). Prenatal residential proximity to agricultural pesticide use and IQ in 7-year-old children. *Environmental Health Perspectives* (https://doi.org/10.1289/EHP504)
23. Caramaschi D, Taylor AE, Richmond RC, Havdahl KA, Golding J, Relton CL, Munafò MR, Smith GD, Rai D. (2018). Maternal smoking during pregnancy and autism: using causal inference methods in a birth cohort study. *Translational Psychiatry* 8: 262 (https://doi.org/10.1038/s41398-018-0313-5)
24. von Ehrenstein OS, Ling C, Cui X, Cockburn M, Park AS, Yu F, Wu J, Ritz B. (2019). Prenatal and infant exposure to ambient pesticides and autism spectrum disorder in children: population based case-control study. 364:l962 (https://doi.org/10.1136/bmj.l962) 364:l962
25. Ongono JS, Béranger R, Baghdadli A, Mortamais M. (2020) Pesticides used in Europe and autism spectrum disorder risk: can novel exposure hypotheses be formulated beyond organophosphates, organochlorines, organochlorines, pyrethroids and carbamates? – A systematic review. Environmental Research 187: 209646 (https://doi.org/10.1016/j.envres.2020.109646)
26. Nicolini C, Fahnestock M. (2018). The valproic acid-induced rodent model of autism. *Experimental Neurology* 299: 217-227 (https://doi.org/10.1016/j.expneurol.2017.04.017)

27. Chaliha D, Albrecht M, Vaccarezza M, Takechi R, Lam V, Al-Salami H, Mamo J. (2020) A systematic review of the valproic acid-induced rodent model of autism. *Developmental Neuroscience* 42:12–48 (https://doi.org/10.1159/000509109)
28. Zerbi V, Pagani M, Markicevic M, Matteoli M, Pozzi D et al. (2021). Brain mapping across 16 autism mouse models reveals a spectrum of functional connectivity subtypes. *Molecular Psychiatry* 26: 7610–7620 (https://doi.org/10.1038/s41380-021-01245-4)
29. Vallortigara G, Regolin L, Marconato F. (2005). Visually inexperienced chicks exhibit spontaneous preference for biological motion patterns. *Plos Biology* 3: e208 (https://doi.org/10.1371/journal.pbio.0030208)
30. Vallortigara G, Regolin L. (2006). Gravity bias in the interpretation of biological motion by inexperienced chicks. *Current Biology* 16: R279-R280 (https://doi.org/10.1016/j.cub.2006.03.052)
31. Johansson G. (1973). Visual perception of biological motion and a model for its analysis. *Perception & Psychophysics* 14: 201-211 (https://doi.org/10.3758/BF03212378)
32. Hadad B, Schwartz S, Mauer D, Lewis TL. (2015). Motion perception: a review of developmental changes and the role of early visual experience. *Frontiers in Integrative Neuroscience* 9: 49 (https://doi.org/10.3389/fnint.2015.00049)
33. Nunes AR, Carreira L, Anbalagan S, Blechman J, Levkowitz G, Oliveira RF. (2020). Perceptual mechanisms of social affiliation in zebrafish. *Scientific Reports* 10: 3642 (https://doi.org/10.1038/s41598-020-60154-8)
34. Dittrich WH, Lea SEG, Barrett J, Gurr PR. (1998). Categorization of natural movements by pigeons: visual concept discrimination and biological motion. *Journal of Experimental Analysis of Behavior* 70:281–299 (https://doi.org/10.1901/jeab.1998.70-281)
35. Blake R. (1993). Cats perceive biological motion. *Psychological Science* 4:54–57 (https://doi.org/10.1111/j.1467-9280.1993.tb00557.x)
36. MacKinnon LM, Troje NF, Dringenberg HC. (2010). Do rats (*Rattus norvegicus*) perceive biological motion? *Experimental Brain Research* 205:571–576 (https://doi.org/10.1007/s00221-010-2378-0)
37. Parron C, Deruelle C, Fagot J. (2007). Processing of biological motion point-light displays by baboons (Papio papio). *Journal of Experimental Psychology: Animal Behavior Processes* 33:381–391 (https://doi.org/10.1037/0097-7403.33.4.381)
38. Tomonaga, M. (2001). Visual search for biological motion patterns in chimpanzees (*Pan troglodytes*). *Psychologia: An International Journal of Psychology in the Orient* 44: 46–59
39. Miura M, Matsushima T. (2012). Preference for biological motion in domestic chicks: sex-dependent effect of early visual experience. *Animal Cognition* 15: 871-879. (https://doi.org/10.1007/s10071-012-0514-x)
40. Miura M, Matsushima T. (2016). Biological motion facilitates imprinting. *Animal Behaviour* 116: 171-180 (https://doi.org/10.1016/j.anbehav.2016.03.025)
41. Miura M, Nishi D, Matsushima T. (2020). Combined predisposed preferences for colour and biological motion make robust development of social attachment through imprinting. *Animal Cognition* 23: 169-188 (doi https://doi.org/10.1007/s10071-019-01327-5)
42. Pavlova M, Sokolov A. (2000). Orientation specificity in biological motion

perception. *Perception & Psychophysics* 62: 889–899 (https://doi.org/10.3758/BF03212075)
43. Troje NF, Westhoff C. (2006). The inversion effect in biological motion perception: evidence for a "life detector"? *Current Biology* 16: 821-824 (https://doi.org/10.1016/j.cub.2006.03.022)
44. The Avian Brain Nomenclature Consortium. (2005). Avian brains and a new understanding of vertebrate brain evolution. *Nature Reviews Neuroscience* 6: 151-159 (https://doi.org/10.1038/nrn1606)
45. Shimizu T, Watanabe S. (2012). The avian visual system. In: How animals see the world: comparative behavior, biology, and evolution of vision. (eds by Olga F. Lazareva, Toru Shimizu, and Edward A. Wasserman) Oxford University Press (https://doi.org/10.1093/acprof:oso/9780195334654.003.0025)
46. Pavlova MA. (2012). Biological motion processing as a hallmark of social cognition. *Cerebral Cortex* 22:981-995. (https://doi.org/10.1093/cercor/bhr156)
47. Chang DHF, Ban H, Ikegaya Y, Fujita I, Troje NF. (2018). Cortical and subcortical responses to biological motion. *Neuroimage* 174: 87-96 ()
48. Hirai M, Senju A. (2020). The two-process theory of biological motion processing. *Neuroscience and Biobehavioral Reviews* 111: 114-124. (https://doi.org/10.1016/j.neubiorev.2020.01.010)
49. Inagaki M, Inoue KI, Tanabe S, Kimura K, Takada M, Fujita I. (2022). Rapid processing of threatening faces in the amygdala of non-human primates: subcortical inputs and dual roles. *Cerebral Cortex* 00:00-00 (https://doi.org/10.1093/cercor/bhac109)
50. Dendrinos G, Hemelt M, Keller A. (2011). Prenatal VPA exposure and changes in sensory processing by the superior colliculus. *Frontiers in Integrative Neuroscience* 5: 68 (https://doi.org/10.3389/fnint.2011.00068)
51. Jure R. (2019). Autism pathogenesis: the superior colliculus. *Frontiers in Neuroscience* 12: 1029 (https://doi.org/10.3389/fnins.2018.01029)
52. Nishigori H, Kagami K, Takahashi A, Tezuka Y, Sanbe A, Nishigori H. (2013). Impaired social behavior in chicks exposed to sodium valproate during the last week of embryogenesis. *Psychopharmacology* 227: 393-402 (https://doi.org/10.1007/s00213-013-2979-y)
53. Sgadò P, Rosa-Salva O, Versace E, Vallortigara G. (2019). Embryonic exposure to valproic acid impairs social predispositions of newly-hatched chicks. *Scientific Reports* 8:5919 (https://doi.org/10.1038/s41598-018-24202-8)
54. Lorenzi E, Pross A, Rosa-Salva O, Versace E, Sgadò P, Vallortigara G. (2019). Embryonic exposure to valproic acid affects social predispositions for dynamic cues of animale motion in newly-hatched chicks. *Frontiers in Physiology* 10: 501 (https://doi.org/10.3389/fphys.2019.00501)
55. Phiel CJ, Zhang F, Huang EY, Guenther MG, Lazar MA, Klein PS. (2001). Histone deacetylase is a direct target of valproic acid, a potent anticonvulsant, mood stabilizer, and teratogen. *Journal of Biological Chemistry* 28: 36734–36741 (https://doi.org/10.1074/jbc.M101287200)
56. Bekoff A, Stein PSG, Hamburger V. (1975). Coordinated motor output in the hindlimb of the 7-day chick embryo. *Proceedings of the National Academy of Sciences of the United States of America* 72: 1245-1248 (https://doi.org/10.1073/pnas.72.4.1245)

57. Bekoff A. (2001). Spontaneous embryonic motility: an enduring legacy. International Journal of Developmental Neuroscience 19: 155-160 (https://doi.org/10.1016/S0736-5748(00)00089-7)
58. Blankenship AG, Feller MB. (2010). Mechanisms underlying spontaneous patterned activity in developing neural circuits. *Nature Reviews Neuroscience* 11: 18-29 (https://doi.org/10.1038/nrn2759)
59. Ben-Ari Y. (2002). Excitatory actions of GABA during development: the nature of the nurture. *Nature Reviews Neuroscience* 3: 728-739 (https://doi.org/10.1038/nrn920)
60. Represa A, Ben-Ari Y. (2005). Tropic actions of GABA on neuronal development. *Trends in Neuroscience* 28: 278-283 (https://doi.org/10.1016/j.tins.2005.03.010)
61. Ben-Ari Y, Gaiarsa JL, Tyzio R, Khazipov R. (2007). GABA: A pioneer transmitter that excites immature neurons and generates primitive oscillations. Physiological Reviews 87: 1215–1284 (https://doi.org/10.1152/physrev.00017.2006)
62. Casile A, Giese MA. (2006). Nonvisual motor training influences biological motion perception. *Current Biology* 16: 69-74 (https://doi.org/10.1016/j.cub.2005.10.071)
63. Jack A, Keifer CM, Pelphrey KA. (2017) Cerebellar contributions to biological motion perception in autism and typical development. *Human Brain Mapping* 38:1914-1932 (https://doi.org/10.1002/hbm.23493)
64. Suzuki Y, Musashi H, Tazawa H. (1989). Noninvasive heart rate monitoring system for avian embryos based on the ballistocardiogram. *Medical and Biological Engineering & Computing* 27: 399-404
65. Scheller M, Bufler J, Hertle I, Schneck H, Franke C, Kochs E. (1996). Ketamine blocks currents through mammalian nicotinic acetylcholine receptor channels by interaction with both the open and the closed state. *Anesthesia & Analgesia* 83: 830-836 (https://doi.org/10.1097/00000539-199610000-00031)
66. Friederich P, Dybek A, Urban BW. (2000). Stereospecific interaction of ketamine with nicotinic acetylcholine receptors in human sympathetic ganglion-like SH-SY5Y cells. *Anesthesiology* 93: 818-824 (https://doi.org/10.1097/00000542-200009000-00032)
67. Harper AA, Rimmer K, Dyavanapalliac J, McArthur JR, Adams DJ. (2020). Ketamine inhibits synaptic transmission and nicotinic acetylcholine receptor-mediated responses in rat intracardiac ganglia in situ. *Neuropharmacology*165: 107932 (https://doi.org/10.1016/j.neuropharm.2019.107932)
68. McMillan R, Muthukumaraswamy SD. (2020). The neurophysiology of ketamine: an integrative review. *Reviews in the Neurosciences* 31: 457-503. (https://doi.org/10.1515/revneuro-2019-0090)
69. Courchesne E, Carper R, Akshoomoff N. (2003). Evidence of brain overgrowth in the first year of life in autism. *Journal of American Medical Association*, 290: 337-344 (https://doi.org/10.1001/jama.290.3.337)
70. Klein S, Sharifi-Hannauer P, Martinez-Agosto JA. (2013). Macrocephaly as a clinical indicator of genetic subtypes in autism. *Autism Research* 6: 51-56 (https://doi.org/10.1002/aur.1266)
71. Barnard-Brak L, Sulak T, Hatz JKI. (2011). Macrocephaly in children with autism spectrum disorders. *Pediatric Neurology* 6: 97-100 (https://doi.org/10.1016/j.pediatrneurol.2010.09.011)
72. Luksch H, Cox K, Karten H. (1998). Bottlebrush dendritic ending and large

dendritic fields: motion-detecting neurons in the tectofugal pathway. *Journal of Comparative Neurology* 396: 399-414 (https://doi.org/10.1002/1096-9861(20000724)423:2<243::AID-CNE5>3.0.CO;2-5)
73. Horn G. (2004). Pathway of the past: the imprint of memory. Nature Reviews Neuroscience 5: 108-120 (https://doi.org/10.1038/nrn1324)
74. Nakamori T, Maekawa F, Sato K, Tanaka K, Ohki-Hamazaki H. (2013). Neural basis of imprinting behavior in chicks. *Development, Growth & Differentiation* 55: 198-206 (https://doi.org/10.1111/dgd.12028)
75. Lorenz K. (1937). The companion in the bird's world. *Auk* 54: 245–273 (https://doi.org/10.2307/40780 77)
76. Morton J, Johnson MH. (1991). CONSPEC and CONLERN: a two-process theory of infant face recognition. *Psychological Review* 98: 164-181 (https://doi.org/10.1037/0033-295X.98.2.164)
77. Yamaguchi S, Aoki N, Kitajima T, Iikubo E, Katagiri S, Matsushima T, Homma KJ. (2012). Thyroid hormone determines the start of the sensitive period of imprinting and primes later learning. *Nature Communications* 3: 1081 (https://doi.org/10.1038/ncomms2088)
78. Batista G, Johnson JL, Dominguez E, Costa-Mattioli M, Pena JL. (2018). Regulation of filial imprinting and structural plasticity by mTORC1 in newborn chickens. *Scientific Reports* 8:8044 (https://doi.org/10.1038/s41598-018-26479-1)
79. Batista G, Hensch TK. (2019). Critical period regulation by thyroid hormones: potential mechanisms and sex-specific aspects. *Frontiers in Molecular Neuroscience* 12:77 (https://doi.org/10.3389/fnmol.2019.00077)
80. Miura M, Aoki N, Yamaguchi S, Homma K-J, Matsushima T. (2018). Thyroid hormone sensitizes the imprinting-associated induction of biological motion preference in domestic chicks. *Frontiers in Physiology (Avian Physiology)* 9:1740 (https://doi.org/10.3389/fphys.2018.01740)
81. Takemura Y, Yamaguchi S, Aoki N, Miura M, Homma KJ, Matsushima T. (2018). Gene expression of Dio2 (thyroid hormone converting enzyme) in telencephalon is linked with predisposed biological motion preference in domestic chicks. *Behavioural Brain Research* 349: 25-30 (https://doi.org/10.1016/j.bbr.2018.04.039)
82. Lorenzi E, Lemaire BS, Versace E, Matsushima T, Vallortigara G. (2021). Resurgence of an inborn attraction for animate objects via thyroid hormone T_3. *Frontiers in Behavioral Neuroscience* 15: 675994 (https://doi.org/10.3389/fnbeh.2021.675994)
83. Lemche E. (2020). Research evidence from studies on filial imprinting, attachment, and early life stress: a new route for scientific integration. *Acta ethologica* 23: 127-133 (https://doi.org/10.1007/s10211-020-00346-7)
84. Knudsen E. (2002). Instructed learning in the auditory localization pathway of the barn owl. *Nature* 417: 322-328 (https://doi.org/10.1038/417322a)
85. Isa T, Marquez-Legorreta E, Grillner S, Scott EK. (2021). The tectum/superior colliculus as the vertebrate solution for spatial sensory integration and action. *Current Biology* 31, R741–R762 (https://doi.org/10.1016/j.cub.2021.04.001)
86. Basso MA, Bickford ME, Cang J. (2021). Unraveling circuits of visual perception and cognition through the superior colliculus. *Neuron* 109: 918-937 (https://doi.org/10.1016/j.neuron.2021.01.013)
87. Zahler SH, Taylor DE, Wong JY, Adams JM, Feinberg EH. (2021). Superior

colliculus drives stimulus-evoked directionally biased saccades and attempted head movements in head-fixed mice. *eLife* 10: e73081. (https://doi.org/10.7554/eLife.73081)
88. Feinberg EH, Meister M. (2015). Orientation columns in the mouse superior colliculus. *Nature* 519: 229-232 (https://doi.org/10.1038/nature14103).
89. Solié C, Contestabile A, Espinosa P, Musardo S, Bariselli S, Huber C, Carleton A, Bellone C. (2022). Superior collicuclus to VTA pathway controls orienting response and influences social interaction in mice. *Nature Communications* 13: 817 (https://doi.org/10.1038/s41467-022-28512-4)
90. Hornix BE, Havekes R, Kas MJH. (2019). Multisensory cortical processing and dysfunction across the neuropsychiatric spectrum. *Neuroscience and Biobehavioral Reviews* 97: 138-151 (https://doi.org/10.1016/j.neubiorev.2018.02.010).
91. Sprengers JJ, van Andel, Zuithoff PA, Keijzer-Veen MG, Schulp AJA, Scheepers FE, Lilien MR, Oranje B, Bruining H. (2021). Bumetanide for core symptoms of autism spectrum disorder (BAMBI): a single center, double-blinded, participant-randomized, plracebo-controlled, phase-2 superiority trial. *Journal of the Americal Academy of Child & Adolescent Psychiatry* 60: 865-876 (https://doi.org/10.1016/j.jaac.2020.07.888)
92. Lemonnier E, Degrez C, Phelep M, Tyzio R, Josse F, Grandgeorge M, Hadjikhani N, Ben-Ari Y. (2012). A randomized controlled trial of bumetanide in the treatment of autism in children. *Translational Psychiatry* 2: e202 (https://doi.org/10.1038/tp.2012.124)
93. Lemonnier E, Villeneuve N, Sonie S, Serret S, Rosier A, Roue M, Brosset P, Viellard M, Bernoux D, Rondeau S, Thummler SD, Ravel D, Ben-Ari Y. (2017). Effects of bumetanide on neurobehavioral function in children and adolescents with autism spectrum disorders. Translational Psychiatry 7: e1056 (https://doi.org/10.1038/tp.2017.10)
94. Aoki N, Yamaguchi S, Matsushima T, Homma KJ. (2018). GABA-A and GABA-B receptors in filial imprinting linked with opening and closing of the sensitive period in domestic chicks (*Gallus gallus domesticus*). *Frontiers in Physiology* (https://doi.org/10.3389/fphys.2018.01837)
95. Hensch TK, Fagiolini M, Mataga N, Stryker MP, Baekkeskov S, Kash S. (1998). Local GABA circuit control of experience-dependent plasticity in developing visual cortex. Science 282: 1504-1508 (ttps://doi.org/10.1126/science.282.5393.1504)
96. Hensch TK. (2018). Critical periods in cortical development. In: The neurobiology of brain and behavioral development. pp: 133-151 (https://doi.org/10.1016/B978-0-12-804036-2.00006-6)
97. Liu Z, Neff RA, Berg DK. (2006). Sequential interplay of nicotinic and GABAergic signaling guides neuronal development. *Science* 314: 1610-1613 (https://doi.org/10.1126/science.1134246)
98. Liu Z, Zhang J, Berg DK. (2007). Role of endogenous nicotinic signaling in guiding neuronal development. *Biochemical Pharmacology* 74: 1112-1119 (https://doi.org/10.1016/j.bcp.2007.05.022)
99. Dwyer JB, McQuown SC, Leslie FM. (2009). The dynamic effects of nicotine on the developing brain. *Pharmacology & Therapeutics* 122: 125-139 (https://doi.org/10.1016/j.pharmthera.2009.02.003)
100. Karvat G, Kimchi T. (2014). Acetylcholine elevation relieves cognitive rigidity and

social deficiency in a mouse model of autism. *Neuropsychophamacology* 39: 831-840. (https://doi.org/10.1038/npp.2013.274)
101. Marotta R, Risoleo MC, Messina G, Parisi L, Carotenuto M, Vetri L, Roccella M. (2020). The neurochemistry of autism. *Brain Sciences* 10: 163 (https://doi.org/10.3390/brainsci10030163)
102. Dineley KT, Pandya AA, Yakel JL. (2015). Nicotine Ach receptors as therapeutic targets in CNS disorders. *Trends in Pharmacological Sciences* 36: 96-108 (https://doi.org/10.1016/j.tips.2014.12.002)
103. Mesulam MM, Mufson EJ, Wainer BH, Levey AI. (1983). Central cholinergic pathways in the rat: an overview based on an alternative nomenclature (Ch1-Ch6). *Neuroscience* 10: 1185-1201 (https://doi.org/10.1016/0306-4522(83)90108-2)
104. Millar NS, Gotti C. (2009). Diversity of vertebrate nicotinic acetylcholine receptors. *Neuropharmacology* 56: 237-246 (https://doi.org/10.1016/j.neuropharm.2008.07.041)
105. Fisher SK, Wonnacott S. (2012). Acetylcholine. In: Basic Neurochemistry, 8th edition. (eds: Brady ST et al.) Elsevier Masson pp.258-282. (https://doi.org/10.1016/B978-0-12-374947-5.00013-4)
106. Ahmed NY, Knowles R, Dehorter N. (2019). New insights into cholinergic neuron diversity. *Frontiers in Molecular Neuroscience* 12: 204 (https://doi.org/10.3389/fnmol.2019.00204)
107. Wang Y, Luksch H, Brecha NC, Karten HJ. (2005). Columnar projections from the cholinergic nucleus isthmi to the optic tectum in chicks (*Gallus gallus*): A possible substrate for synchronizing tectal channels. *Journal of Comparative Neurology* 494: 7-35 (https://doi.org/10.1002/cne.20821)
108. Asadollahi A, Mysore SP, Knudsen EI. (2010). Stimulus-driven competition in a cholinergic midbrain nucleus. *Nature Neuroscience* 13: 889-895 (https://doi.org/10.1038/nn.2573)
109. Knudsen EI. (2011). Control from below: the role of a midbrain network in spatial attention. *European Journal of Neuroscience* 33: 1961–1972 (https://doi.org/10.1111/j.1460-9568.2011.07696.x)
110. IImura K, Suzuki H, Hotta H. (2019). Thyroxin and calcitonin secretion into thyroid venous blood is regulated by pharyngeal mechanical stimulation in anesthetized rats. *Journal of Physiological Sciences* 69: 749-756 (https://doi.org/10.1007/s12576-019-00691-8)
111. Román GC, Ghassabian A, Bongers-Schokking JJ, Jaddoe VWV, Hofman A, de Rijke YB, Verhult FC, Tiemeir H. (2013). Association of gestational maternal hypothyroxinemia and increased autism risk. *Annals of Neurology* 74: 733-742 (https://doi.org/10.1002/ana.23976)
112. Berbel P, Navarro D, Román GC. (2014). An evo-devo approach to thyroid hormones in cerebral and cerebellar cortical development: etiological implications for autism. *Frontiers in Endocrinology* 5: 146 (https://doi.org/10.3389/fendo.2014.00146)
113. Getahun D, Jacobson SJ, Fassett MJ, Wing DA, Xiang AH, Chiu VY, Peltier MR. (2018). Association between maternal hypothyroidism and autism spectrum disorders in children. Pediatric Research 83: 580–588 (https://doi.org/10.1038/pr.2017.308)
114. Hallmann CA, Foppen RPB, van Turnhaut CAM, de Kroon H, Jongejans E. (2014).

Declines in insectivorous birds are associated with high neonicotinoid concentration. *Nature* 511: 341-343 (https://doi.org/10.1038/nature13531)
115. Eng ML, Stutchbury BJM, Morrissey CA. (2017). Imidacloprid and chlorypyrifos insecticides impair migratory ability in a seed-eating songbird. *Scientific Reports* 7: 15176 (https://doi.org/10.1038/s41598-017-15446-x)
116. Eng ML, Stutchbury BJM, Morrissey CA. (2019). A neonicotinoid insecticide reduces fueling and delays migration in songbirds. *Science* 365: 1177-1180 (https://doi.org/10.1126/science.aaw9419)
117. Gunier RB, Bradman A, Harley KG, Kogut K, Eskenazi B. (2017). Prenatal residential proximity to agricultural pesticides use and IQ in 7-year-old children. *Environmental Health Perspectives* 125: 5 (https://doi.org/10.1289/EHP504)
118. Ikenaka Y, Miyabara Y, Ichise T, Nakayama S, Nimako C, Ishizuka M, Tohyama C. (2018). Exposures of children to neonicotinoids in pine wilt disease control areas. *Environmental Toxicology & Chemistry* 38: 71-79 (https://doi.org/10.1002/etc.4316)
119. von Ehrenstein OS, Ling C, Cui X, Cockburn M, Park AS, Yu F, Wu J, Ritz B. (2019). Prenatal and infant exposure to ambient pesticides and autism spectrum disorder in children: population based case-control study. *the BMJ* 364: 1962 (http://dx.doi.org/10.1136/bmj.l962)
120. Ongono JS, Béranger R, Baghdadli A, Mortamais M. (2020). Pesticides used in Europe and autism spectrum disorder risk: can novel exposure hypotheses be formulated beyond organophosphates, organochlorines, pyrethroids and carbamates? – A systematic review. *Environmental Research* 187: 109646 (https://doi.org/10.1016/j.envres.2020.109646)
121. Sano K, Isobe T, Yang J, Win-Shwe T, Yoshikane M, Nakayama SF, Kawashima T, Suzuki G, Hashimoto S, Nohara K, Tohyama C, Maekawa F. (2016). In utero and lactational exposure to acetamiprid induces abnormalities in socio-sexual and anxiety-related behaviors of male mice. *Frontiers in Neuroscience* 10: 228 (https://doi.org/10.3389/fnins.2016.00228)
122. Bean TG, Gross MS, Karouna-Renier NK, Henry PFP, Schultz SL, Hladik ML, Kuivila KM, Rattner BA. (2019). Toxicokinetics of imidacloprid-coated wheat seeds in Japanese quail (*Coturnix japonica*) and an evaluation of hazard. *Environmental Science & Technology* 53: 3888-3897 (https://doi.org/10.1021/acs.est.8b07062)
123. Willner P. (1984). The validity of animal models of depression. *Psychopharmacology* 83: 1-16 (https://doi.org/10.1007/BF00427414)
124. Belzung C, Lemoine M. (2011). Criteria of validity for animal models of psychiatric disorders: focus on anxiety disorders and depression. *Biology of Mood & Anxiety Disorders* 1: 9 (https://doi.org/10.1186/2045-5380-1-9)
125. Rugani R, Fontanari L, Simoni E, Regolin L, Vallortigara G. (2009). Arithmetic in newborn chicks. *Proceedings of the Royal Society B* 276: 2451-2460 (https://doi.org/10.1098/rspb.2009.0044)
126. Pecchio T, Vallortigara G. (2010). View-based strategy for reorientation by geometry. *Journal of Experimental Biology* 213: 2987-2996 (https://doi.org/10.1242/jeb.043315)
127. Rugani R. (2017). Towards numerical cognition's origin: insights from day-old domestic chicks. *Philosophical Transactions B* 373: 20160509

(https://doi.org/10.1098/rstb.2016.0509)
128. Daisley JN, Vallortigara G, Regolin L. (2021). Low-rank *Gallus gallus domesticus* chicks are better at transitive inference reasoning. Communications Biology 4: 1344 (https://doi.org/10.1038/s42003-021-02855-y)
129. Lemaire BS, Rucco D, Josserand M, Vallortigara G, Versace E. (2021). Stability and individual variability of social attachment in imprinting. *Scientific Reports* 11: 7914 (https://doi.org/10.1038/s41598-021-86989-3)
130. Szabó E, Chiandetti C, Téglás E, Versace E, Csibra G, Kovács ÁM, Vallortigara G. (2022). Young domestic chicks spontaneously represent the absence of objects. *eLife* 11: e67208 (https://doi.org/10.7554/eLife.67208)
131. Hemmings NL, Slate J, Birkhead TR. (2012). Inbreeding causes early death in a passerine bird. Nature Communications 3: 863 (https://doi.orgMa10.1038/ncomms1870)

Supplementary materials: Methods and Statistical Analyses

1. Methods

1.1.Animals and compliance with ethical standard

Experiments were conducted under the guidelines and approval of the Committee on Animal Experiments of Hokkaido University (approval number 20-0141). The guidelines are based on the national regulations for animal welfare in Japan (Law for Humane Treatment and Management of Animals, after partial amendment No. 68, 2005). Number of subjects used are indicated below in the statistical analyses for each experiment.

Domestic white Leghorn chicks (*Gallus gallus domesticus*, an egg-laying strain of Leghorn called "Julia") were used. Fertilized eggs were purchased from a local hatchery (Iwamura Co., Niigata/Hokkaido Japan) every 2 weeks, and the batch was numbered. Eggs were incubated in the laboratory by using type P-008B incubators (Showa Furanki Co., Saitama Japan) with its temperature controlled at 37.7°C and the humidity at ca. 80%. The inside of the incubator was kept in complete darkness until hatch. Chicks were individually hatched in small boxes separated by black plastic walls, so that they could interact acoustically but not visually. To avoid post-hatch visual experiences, hatchlings were individually housed in boxes placed in another incubator of the same type, kept in darkness until the experiment. Chicks were sexed after the experiment. Generally, fertilized eggs weighed 59.8 ± 3.1 g (mean ± s.d., n=170) and ca. 2 g lighter at embryonic 14 days (E14) whereas the shells weighed 8.0 ± 0.1 g (n=16), so that the wet weight is assumed to be around 50 g. In this series of experiments, as the egg weight did not considerably vary, the amount of injected chemical per egg was fixed and not adjusted for each egg.

1.2. Ballistographic recording of embryonic movements (experiment 1)

Mechanical vibration caused by spontaneous fetal movements were recorded following the ballistocardiogram method developed by Suzuki et al. (1989). By a micromanipulator, an analog record stylus cartridge (type AT VM95E, Audio Technica Co., Tokyo Japan) was gently pushed against the shell of egg placed on a thin rubber membrane, which was stretched on a glass jar (**Fig.1A**). The jar and the manipulator were firmly settled on a heavy iron plate and housed in a constant temperature incubator at 37.7°C and high humidity. The recorded monoaural signal was amplified by a hand-made low input-impedance amplifier (made of FET operational amplifier, TL084), band-pass filtered (cut-off frequency: 10~100Hz, magnification: x1,000), and stored at 1,000 point/sec sampling rate by Spike2 (ver.7, the interface CED-1401 micro3, Cambridge Electric Design Co., Cambridge UK). Frequency spectrum of 2-20 Hz range was monitored, and the converted power was stored at every 1 sec (**Fig.1B**). Using R as platform (see below), the power value was averaged at every 1 min, and the temporal profiles were constructed for pre-injection 30 min and post-injection 90 min for each egg.

1.3.Apparatus and procedures of imprinting and tests (experiment 2,3,4)

An I-shaped maze (10 cm wide, 70 cm long) was equipped with a 50-cm-long treadmill consisting of a rubber belt at the center and an LCD monitor at each end (**Fig.1C**) and placed in a dark room at 27~28°C. See our previous reports for details

(Miura et al., 2018, 2020; Takemura et al. 2018). Two training sessions (1 hour each) were given at 1 hour interval. An infrared sensor and a transparent Plexiglass partition were placed at a point 10 cm from one monitor, and the other monitor was occluded by an opaque partition. A loudspeaker behind the LCD monitor emitted mechanical sound synchronized with the toy movement on the screen. When chicks approached the monitor and hit the sensor, the rubber belt of the treadmill moved for a short period of 0.3 s, drawing the chick backward by about 30 cm at a time with the shortest intervals set at 0.1~1 sec. The apparatus was controlled by Arduino®. The treadmill motions were digitally counted, and the number of approaches was recorded for each chick. We monitored the chick behavior via a video camera set at the ceiling.

After 30 min to 1 hour pause period in a dark chamber kept at ~30°C, the trained chicks were tested in binary choice using the same apparatus without treadmill motions. In the BM test, one monitor displayed a linear point-light animation and the other monitor a walking one, both composed of white lights. In the subsequent imprinting test, one monitor displayed red toy (familiar object) and another yellow (novel object), both unaccompanied by the mechanical sound used in training. We consider that the subject chose one side when the whole body was located close (<30 cm) to the monitor (delineated by dashed line). Five-min tests were repeated twice after swapping the side, and the initial side was also counterbalanced among individuals. Tests were video-recorded. Intervals between test trials were set at 90-120sec. The difference in stay times gave the choice score in sec thus ranging in -600 to +600 sec.

In experiment 2, chicks were trained and tested on post-hatch 1 day (P1, at 12~36 hours after hatch) by the procedure shown in **Fig.1C**. In experiment 3, chicks were similarly trained and tested for the BM preference on P1, then re-trained by merged Lp(red) and Wp(yellow) on P2 (**Fig.2C**); the chicks were simultaneously exposed to two point-light animations, one walking in yellow Wp(yellow) and another linear in red Lp(red). Our recent study (Miura et al. 2020) revealed that chicks exposed to the merged animations showed significantly higher preference to Wp(yellow) over Lp(red), if the BM preference of the chicks had been induced by the training using the red toy on P1.

1.4. Video clips and point-light animations for training and tests

Two video clips of a rotating toy and 3 point-light animations were prepared as in our previous reports (Miura and Matsushima 2016, Miura et al. 2018, 2020); see below for the list. Video clips were displayed on black background at a speed of 30 frames/s. We made editing by Adobe Premiere (Elements 7) and the color was set either to red (R: 255, G: 0, B: 0) or yellow (R: 255, G: 255, B: 0). These stimuli were displayed on the LCD monitors (size 10.4”, 800 × 600 pixels, Logitec LCM-T102AS, Japan; flash rate: 56–75 Hz, brightness: 230 cd/m2, pitch size: 0.264 × 0.264 mm) using free viewer software (A-player, version 6.0) on PC. The width of the presentation was set at 10.5 cm on the monitor, the surface of which was placed at 2.0 cm away from the terminal window of the maze.

Moving-toy(red).wmv	P1 training and imprinting test (experiment 2,4)
Moving-toy(yellow).wmv	imprinting test (experiment 2,4)
Wp(white).wmv	BM test (experiment 2,4)
Lp(white).wmv	BM test (experiment 2,4)
Wp(yellow)-Lp(red).wmv	P2 training (experiment 4)

Wp(yellow).wmv	imprinting_1 (biological) test (experiment 4)
Lp(red).wmv	imprinting_1 (biological) test (experiment 4)

1.5.Chemical agents

Eggs (embryonic 14 days, E14, if not stated otherwise) received single injection of 200μL solution to the air chamber through one of two holes on the round edge of the shell; another hole served as air vent for smooth injection. The holes were sealed by mending tape. For each agent, the highest dosage was determined which (1) did not reduce the rate of hatching and (2) significantly suppressed the spontaneous fetal motions, then 1/5 diluted solution was tested. Control eggs received injection of the same amount of vehicle, distilled water.

name, code and company of the chemical agents

chemical name	code number	company
VPA (sodium valproate)	cas no.1069-66-5	FUJIFILM Wako Pure Chemical Co.
ketamine (hydrochloride)	ATC code N01AX03	Daiichi-Sankyo Propharma Co.
mk801 ((+)-mk801 maleate)	cas no. 77086-22-7	FUJIFILM Wako Pure Chemical Co.
tubocurarine (D-tubocurarine chloride pentahydrate)	cas no. 41354-45-4	FUJIFILM Wako Pure Chemical Co.
MLA (methyllycaconitine citrate)	cas no. 112825-05-5	abcam
DHβE (dihydro-β-erythroidine hydrobromide)	cas no. 29734-68-7	TOCRIS Biocscience
imidacloprid (standard)	cas no. 105827-78-9	FUJIFILM Wako Pure Chemical Co.
bumetanide	cas no. 28395-03-1	TOCRIS Bio-techne
VU0463271	cas no. 1391737-01-1	TOCRIS Neuroscience

amount of agents injected / egg ~ 50g

chemical agent	molecular weight	μmole
VPA 5.82mg	166.19	35.0
ketamine 0.20mg	274.19	0.729
mk801 0.25mg	337.37	0.741
tubocurarine 0.20mg	771.72	0.259
MLA 0.15mg	874.92	0.171
DHβE 0.15mg	356.26	0.421
imidacloprid 0.05mg	255.66	0.196
bumetanide 0.02mg	364.42	0.0549
VU0463271 0.2mg	387	0.517

1.6.Histone acetylation assay in cultured brain cells (experiment 5)

Embryos (E7 and E14) were aseptically harvested from eggs and brain tissues were separated. Brain tissues were finely minced with scissors in sterile phosphate-buffered saline (PBS) and dissociated by pipetting with micropipette tips. Dissociated brain tissues were suspended in a brain culture medium composed of DMEM/F12 (048-29785, FUJIFILM Wako Pure Chemical Co., Tokyo, Japan), 10% foetal bovine serum (S-FBS-NL-015, Serana Europe GmbH, Brandenburg, Germany), 1x Antibiotic-Antimycotic (15240-096, Life Technologies Co., CA, USA), and maintained on coverslip glasses coated with collagen type I-C (631-00771, FUJIFILM Wako Pure Chemical Co., Tokyo, Japan) for 4 days at 37°C in 5% CO_2 condition.

The cultured brain tissues were incubated with ketamine (66 or 6.6 μg/mL), VPA (1.2 mM or 0.12 mM) or vehicle PBS in a brain culture medium without FBS for 2 hours at 37°C in 5% CO_2. After incubation, cultured brain tissues were fixed with 4% paraformaldehyde in PBS for 5 mins, blocked with a blocking solution (4% normal goat serum (S-1000, VECTOR laboratories Inc., CA, USA), 1% blocking reagent (1096176, Roche Ltd., Basel, Swiss) and 0.5% Tween20 in PBS) for 30 mins, and then incubated with 1:3000 diluted Anti-acetyl Histone H3 (Lys27), mouse monoclonal antibody (MA309A, TaKaRa Bio Inc., Shiga, Japan) in the blocking solution for 16 hours at 4°C in a humidity chamber. Following the first antibody incubation, tissues were incubated with 1:2000 diluted Goat anti-Mouse IgG, Alexa Fluor 555 antibody (A21422, ThermoFisher Scientific, MA, USA) in the blocking solution for 2 hours at room temperature in a humidity chamber. Stained tissues were mounted in Mounting Medium with DAPI (H-1200, VECTOR Laboratories Inc.) and imaged using a BZ-X810 microscope (Keyence Co., Osaka, Japan). In each duplicated experimental group, three fields of view were taken per coverslip, and the acetylation level of H3K27 in the nuclei of 100 randomly selected cells from six fields of view was measured as fluorescence intensity using Image J.

1.7.Brain weight and isotropic fractionator measurement of brain cells (experiment 6)

The P1 chicks were transcardially perfused by 4% paraformaldehyde in 0.1M phosphate buffer under a deep anesthesia by i.m. injection of 0.8mL ketamine-xylazine cocktail; a 1:1 mixture of 10mg/mL ketamine hydrochloride (Daiichi-Sankyo Propharma Co.) and 2mg/mL xylazine (Sigma-Aldrich Co.).

The whole brain (cut at the caudal end of medulla oblongata) was dissected and post-fixed in the fixative for overnight, stored for 2~4 days in phosphate-buffered saline (PBS) at 4°C and weighed. The telencephalon was isolate at the rostral level of diencephalon and manually chopped in small pieces by scalpel. The tissue was weighed and homogenized in a detergent solution (40mM sodium citrate and 1% Triton X-100) using a 7mL glass Tenbroeck tissue homogenizer. The homogenate and several washes of the homogenizer were transferred to a 50ml falcon tube using a glass pipette. To visualize cell nuclei DAPI (4,6-diamidino-2-phenylindoledihydrochloride, Invitrogen, Carlsbad, Calif., USA) was added to the suspension from a stock solution at 20 mg/L (dilution 1:20 to 1:50) and the final volume of the suspension was recorded. To estimate the total amount of cells in the suspension, the nuclear density was quantified in a Neubauer chamber by a fluorescent microscope (BX-50, Olympus Co., Tokyo, Japan) according to the protocol developed by Herculano-Houzel and Lent (2005).

To estimate the number of matured neuron, aliquot (500 μL) of the nuclear

suspension washed with PB (0.1M) and incubated overnight in the dark at 4°C with Cy3-labeled rabbit polyclonal neuronal nuclear antigen antibody (1:150 dilution; NeuN, RRID:AB_11204707). The percentage of neuronal nuceli was determined by counting at least 500 DAPI-stained nuclei and establishing the fraction that was also NeuN positive, according to the protocol developed by Herculano-Houzel and Lent (2005). Briefly, the total number of neurons in each sample was determined by multiplying the total number of cells in the structure by the NeuN-positive fraction obtained. The total number of non-neuronal cells was determined by subtracting the total number of neurons from the total number of cells. Densities of neurons and non-neurons (cell/mg) were determined by dividing the number of neurons or non-neurons by the mass (mg) of the structure.

1.8.qPCR analysis of gene expression (experiment 7)

Brain slices (500μm thick, left hemisphere) were prepared from E14, E18 embryos and P1 chicks using a vibrating micro-slicer (DTK-1000, Dosaka EM Co., Kyoto, Japan). Embryos were harvested from eggs, and hatchling were decapitated under a deep anesthesia by ketamine-xylazine. To minimize the sensory stimuli, the eggs were maintained in a dark incubator and the hatchlings were isolated in individual cages kept at 30°C in complete darkness. Slices were collected in ice-chilled PBS, and punchout tissues of 1.5 mm diameter (one piece for each brain region) were manually sampled and immediately frozen.

Total RNA was extracted from the tissues using a column-based method (FastGene RNA Premium Kit; FG-81050, NIPPON Genetics Co. Ltd., Tokyo, Japan), and reverse transcribed into cDNA using random primers and a high-capacity cDNA reverse transcription kit (4368814, ThermoFisher Scientific). The expression levels of genes were analyzed by reverse transcription qPCR with KOD SYBR qPCR mix (QKD-201,TOYOBO Co. Ltd., Nagoya, Japan) and primers; for the list see the table below. The copy number of genes were determined by comparison with standard curves. Standard curves were generated from serial dilution of pGEM-T Easy plasmids (A1360, Promega, USA) inserted with the sequence cloned by the primers.

gene	forward primer (5'-3')	reverse primer (5'-3')
CHRNA4	TTTCGGATGTGGTCCTGGTC	AAGTCACCATCAGCATTGTTGT
CHRNA7	TGCAGATCATGGATGTGGATGA	TGGCAGTGTCCCGAAGAATT
SLC12A2	CCAGATGTGAACTGGGGATCA	TTGCCTCCGAGGACCCATAT
SLC12A5	GGTCTTCCTTTGCTGCTCCT	GGGAAGATGTAGGCCAGCAG
RBFOX3	CCGGGTGATGACGAACAAGA	GTACACTCGGCCGTAACTGT
GAPDH	GCAGATGCAGGTGCTGAGTA	GACACCCATCACAAACATGG

2. Statistical analyses

Statistical computations were performed on RStudio version 3.6.3 (2020-02-29). For single/multiple regression analyses, linear models were constructed using the function *lm()* with the control group as the reference set; one model was calculated for

each set of experimental groups. Multiple regression including variables such as *sex*, *batch* and *run* (locomotor counts during training) appeared not to improve the statistical judgements; we therefore adopted single regression by *drug* (and dose) in most cases.

In experiment 7, where gene expression profiles were examined, IMM and E14 served the reference for the brain region and the age, respectively. Significance is coded as 0 < *** < 0.001 < ** < 0.01 < * <0.05, and ns means p-value ≥ 0.05.

2.1. Experiment 1 (Fig.1C)

ballistography index explained by drug:

fit_exp_1_ballistography_selected <- lm(ratio ~ label, data = dataset_exp_1_ballistograpphy_fig)
summary(fit_exp_1_ballistography_selected)

Coefficients:

label (drug)	estimate	std. error	t-value	Pr(>|t|)	signif. code
(intercept)	+1.18063	0.07899	14.947	< 2e-16	***
VPA 5.82mg	−0.56805	0.13099	−4.337	6.23e-05	***
ketamine 0.20mg	−0.57210	0.13099	−4.368	5.60e-05	***
mk801 0.25mg	−0.69986	0.13099	−5.343	1.80e-06	***
tubocurarine 0.20mg	−0.67630	0.13099	−5.163	3.46e-06	***
MLA 0.15mg	−0.56939	0.13099	−4.347	6.01e-05	***
DHβE 0.15mg	−0.78066	0.13099	−5.960	1.87e-07	***

residual standard error = 0.2956 (Df = 55)
multiple r-squared = 0.5006, adjusted r-squared = 0.4461
F-statistic = 9.188 (Df = 6, 55 DF), p-value = 5.765e-07

2.2 Experiment 2 (Fig.1E)

BM score explained by drug:

fit_exp2_bm_selected <- lm (bm ~ label, data = dataset_exp_2_bm_imprint_fig)
summary (fit_exp2_bm_selected)

Coefficients:

drug	estimate	std. error	t-value	Pr(>|t|)	signif. code
(intercept)	+136.309	16.187	8.421	1.27e-14	***
VPA 5.82mg	+26.091	59.031	0.442	0.65904	ns
ketamine 0.20mg	−146.809	59.031	−2.487	0.01382	*
mk801 0.25mg	−9.509	59.031	−0.161	0.87221	ns
tubocurarine 0.20mg	−162.509	59.031	−2.753	0.00653	**
MLA 0.15mg	−153.509	59.031	−2.600	0.01010	*
DHβE 0.15mg	−50.309	59.031	−0.852	0.39524	ns

residual standard error = 179.5 (Df=176)
multiple r-squared = 0.09761, adjusted r-squared = 0.06685
F-statistic = 3.173 (Df=6, 176), p-value = 0.005568

imprinting score explained by drug:

fit_exp2_imprint_selected <- lm (imprint ~ label, data = dataset_exp_2_bm_imprint_fig)

summary (fit_exp2_imprint_selected)
Coefficients:

drug	estimate	std. error	t-value	Pr(>|t|)	signif. code
(intercept)	+419.52	20.66	20.311	< 2e-16	***
VPA 5.82mg	−316.22	75.33	−4.198	4.27e-05	***
ketamine 0.20mg	−118.62	75.33	−1.575	0.1171	ns
mk801 0.25mg	+3.88	75.33	0.052	0.9590	ns
tubocurarine 0.20mg	+47.08	75.33	0.625	0.5328	ns
MLA 0.15mg	−160.32	75.33	−2.128	0.0347	*
DHβE 0.15mg	−151.02	75.33	−2.005	0.0465	*

residual standard error = 229.1 (DF = 176)
multiple r-squared = 0.1303, adjusted r-squared = 0.1007
F-statistic = 4.396 (DF = 6, 176), p-value = 0.0003639

2.3.Experiment 3 (Fig.2)
ballistography index explained by drug (Fig.2A):
fit_exp_1_ballistography_selected <- lm(ratio ~ label, data = dataset_exp_1_ballistography_imi)
summary(fit_exp_1_ballistography_selected)
Coefficients:

drug	estimate	std. error	t-value	Pr(>|t|)	signif. code
(intercept)	+1.18063	0.08043	14.679	2.17e-14	***
IMI (0.005mg)	−0.28187	0.13337	−2.113	0.043951	*
IMI (0.05mg)	−0.59009	0.13337	−4.424	0.000143	***

residual standard error = 0.3009 (DF = 27)
multiple r-squared = 0.4239, adjusted r-squared = 0.3812
F-statistic =9.934 (DF = 2, 27), p-value = 0.0005842

BM score explained by drug (Fig.2Ba):
fit_exp_3_bm <- lm (bm ~ label, data = dataset_exp_2_bm_imprint_ctrl_imi)
summary (fit_exp_3_bm)
Coefficients:

drug	estimate	std. error	t-value	Pr(>|t|)	signif. code
(intercept)	117.66	21.05	5.589	1.42e-07	***
E0 IMI (0.005mg)	−28.25	47.90	−0.590	0.5564	ns
E0 IMI (0.05mg)	−109.98	45.82	−2.400	0.0179	*
E14 IMI (0.005mg)	−114.16	59.92	−1.905	0.0591	ns
E14 IMI (0.05mg)	−137.06	59.92	−2.288	0.0239	*

residual standard error = 177.4 (DF = 122)
multiple r-squared = 0.08534, adjusted r-squared = 0.05535
F-statistic =2.846 (DF = 4, 122), p-value = 0.02689

imprinting score explained by drug (Fig.2Ba):
fit_exp_3_imprint <- lm (imprint ~ label, data = dataset_exp_2_bm_imprint_ctrl_imi)
summary (fit_exp_3_imprint)
Coefficients:

drug	estimate	std. error	t-value	Pr(>|t|)	signif. code
(intercept)	417.03	28.98	14.390	<2e-16	***
E0 IMI (0.005mg)	+20.74	65.94	0.314	0.754	ns
E0 IMI (0.05mg)	−99.03	63.08	−1.570	0.119	ns
E14 IMI (0.005mg)	−60.13	82.48	−0.729	0.467	ns
E14 IMI (0.05mg)	−101.13	82.48	−1.226	0.223	ns

residual standard error = 244.2 (DF = 122)
multiple r-squared = 0.03378, adjusted r-squared = 0.0021
F-statistic = 1.066 (DF = 4, 122), p-value = 0.3762

2.4.Mahalanobis distance (MD) analysis of Experiment 2 & 3 data

We made post-hoc analysis on the behavioral data of experiments 2 and 3 by considering both BM and imprinting scores as a multi-variance data set. Gravity centers (defined as mean values for BM and imprinting scores) were compared with the control data set as the reference. As the correlation between these two scores was significant in the control dataset (see below; r=0.21, p<0.05), we adopted the Mahalanobis distance (MD; Taguchi and Rajesh 2000) to calculate the distance of experimental group measured from the control gravity center.

Gravity centers (mean values) of BM and imprinting scores

groups (drug)	n	BM score		imprinting score	
		average	s.e.m.	average	s.e.m.
control*	**123**	**136.31**	**16.14**	**419.52**	**20.25**
VPA 5.82mg	10	162.40	83.84	103.30	92.77
ketamine 0.20mg	10	-10.50	59.70	300.90	71.23
mk801 0.25mg	10	126.80	43.78	413.70	70.45
tubocurarine 0.20mg	10	-26.20	51.92	466.60	55.59
MLA 0.15mg	10	-17.20	43.89	259.20	96.56
DHβE 0.15mg	10	86.00	49.65	268.50	65.77
E0 IMI 0.005mg	17	89.41	35.68	437.77	41.82
E0 IMI 0.05mg	19	7.68	27.84	318.00	57.02
E14 IMI 0.005mg	10	3.50	53.57	356.90	103.40
E14 IMI 0.05mg	10	-19.40	53.76	315.90	81.70

*Correlation coefficient and its significance level was given for the control data by:
cor_test(dataset_exp_2_bm_imprint_ctrl, bm, imprint, method = "spearman")
r=0.21, *statistic*=245996.6, p=0.0217

Random sampling of 10 points from the control dataset was repeated 10,000 times, giving rise to the distribution of the sum of MD as shown in the supplementary figure

Fig.S4. Critical levels of the sum of MD_{10} (sum of MD of 10 samples) were thus determined for 90% (black; MD_{10} = 36.57572), 95% (brown; MD_{10} = 42.74558), 99% (red; MD_{10} = 56.81546) and 99.9% (pink; MD_{10} = 76.95151), respectively. The MD distance between each group and the control (origin) is shown below.

groups (drug)	n	MD distance	siginif. code
VPA 5.82mg	10	52.37958	*
ketamine 0.20mg	10	28.35494	ns
mk801 0.25mg	10	11.97952	ns
tubocurarine 0.20mg	10	22.61997	ns
MLA 0.15mg	10	33.41734	ns
DHβE 0.15mg	10	19.22331	ns
E0 IMI 0.005mg#	17	12.70195	ns
E0 IMI 0.05mg#	19	22.40369	ns
E14 IMI 0.005mg	10	28.34648	ns
E14 IMI 0.05mg	10	36.14058	ns

MD distance is normalized by the factor of 10/n.

2.5.Experiment 4 (Fig.3)

BM score explained by drug only (Fig.3B):

fit_exp4_bm_drug <- lm(bm ~ drug, data = dataset_exp_4_double_imprint)
summary (fit_exp4_bm_drug)

Coefficients:

drug	estimate	std. error	t-value	Pr(>|t|)	signif. code
control	145.80	52.24	2.791	0.00781	**
VPA 5.82mg	−18.22	78.37	−0.232	0.81729	ns
ketamine 0.20mg	−172.30	82.61	−2.086	0.04296	*
tubocurarine 0.20mg	−235.00	82.61	−2.845	0.00678	**

residual standard error = 202.3 (DF = 43)
multiple r-squared = 0.2076, adjusted r-squared = 0.1523
F-statistic =3.755 (DF= 3, 43), p-value = 0.01758

imprinting_1 (biological) score explained by drug only (Fig.3C):

fit_exp4_imprint_1 <- lm(imprint_1 ~ drug, data = dataset_exp_4_double_imprint)
summary (fit_exp4_imprint_1)

Coefficients:

drug	estimate	std. error	t-value	Pr(>|t|)	signif. code
control	37.13	59.77	0.621	0.5377	ns
VPA 5.82mg	−213.05	89.66	−2.376	0.0220	*
ketamine 0.20mg	−201.53	94.51	−2.132	0.0387	*
tubocurarine 0.20mg	−60.33	94.51	−0.638	0.5266	ns

residual standard error = 231.5 (DF = 43)
multiple r-squared = 0.1533, adjusted r-squared = 0.09428
F-statistic = 2.596 (DF = 3, 43), p-value = 0.06465

imprinting_1 (biological) score explained by drug and BM score (Fig.3C):

*fit_exp4_imprint_1_bm <- lm(imprint_1 ~ drug * bm, data = dataset_exp_4_double_imprint)*
summary (fit_exp4_imprint_1_bm)
Coefficients:

drug/BM	estimate	std. error	t-value	Pr(>|t|)	signif. code
(intercept)	-128.6864	72.0850	-1.785	0.082007	ns
VPA 5.82mg	-1.7390	99.4170	-0.017	0.986134	ns
ketamine 0.20mg	-36.8073	98.1233	-0.375	0.709609	ns
tubocurarine 0.20mg	104.6133	103.3479	1.012	0.317660	ns
BM	1.1373	0.3286	3.462	0.001317	**
VPA*BM	-1.4939	0.4161	-3.591	0.000911	***
ketamine*BM	-1.1786	0.4706	-2.505	0.016545	*
tubocurarine*BM	-1.1471	0.5003	-2.293	0.027323	*

residual standard error = 208.6 (DF = 39)
multiple r-squared = 0.3764, adjusted r-squared = 0.2645
F-statistic = 3.363 (DF = 7, 39), p-value = 0.00668

imprinting_2 (artifact) score explained by drug only (Fig.3D):
fit_exp4_imprint_2 <- lm(imprint_2 ~ drug, data = dataset_exp_4_double_imprint)
summary (fit_exp4_imprint_2)
Coefficients:

drug	estimate	std. error	t-value	Pr(>|t|)	signif. code
control	487.13	68.66	7.095	9.38e-09	***
VPA 5.82mg	−277.38	102.99	−2.693	0.0100	*
ketamine 0.20mg	−194.93	108.56	−1.796	0.0796	ns
tubocurarine 0.20mg	−91.23	108.56	−0.840	0.4053	ns

residual standard error = 265.9 (DF = 43)
multiple r-squared = 0.1582, adjusted r-squared = 0.09942
F-statistic = 2.693 (DF = 3, 43), p-value = 0.0579

imprinting_2 (artifact) score explained by drug and BM (Fig.3D):
*fit_exp4_imprint_2_bm <- lm(imprint_2 ~ drug*bm, data = dataset_exp_4_double_imprint)*
summary (fit_exp4_imprint_2_bm)
Coefficients:

drug/BM	estimate	std. error	t-value	Pr(>|t|)	signif. code
(intercept)	470.3160	93.4620	5.032	1.13e-05	***
VPA 5.82mg	-320.8333	128.8993	-2.489	0.0172	*
ketamine 0.20mg	-179.5913	127.2220	-1.412	0.1660	ns
tubocurarine 0.20mg	-103.0923	133.9960	-0.769	0.4463	ns
BM	0.1153	0.4260	0.271	0.7880	ns
VPA*BM	0.3570	0.5394	0.662	0.5120	ns
ketamine*BM	-0.1710	0.6101	-0.280	0.7807	ns
tubocurarine*BM	-0.4368	0.6486	-0.673	0.5046	ns

residual standard error = 270.5 (DF = 39)
multiple r-squared = 0.21, adjusted r-squared = 0.06819
F-statistic = 1.481 (DF = 7, 39), p-value = 0.2026

2.6.Experiment 5 (Fig.4A)
H3K27ac fluorescence explained by drug:
fit_exp_5_h3k27ac <- lm(flu ~ drug, data = dataset_exp_5_h3k27ac)
summary(fit_exp_5_h3k27ac)
Coefficients:

drug	estimate	std. error	t-value	Pr(>|t|)	signif. code
(intercept)	+7.4293	0.3156	23.537	<2e-16	***
VPA 0.12mM	+0.5917	0.4464	1.326	0.186	ns
VPA 1.2mM	+11.9921	0.4464	26.865	<2e-16	***
ketamine 6.6 µg/mL	− 0.4920	0.4464	−1.102	0.271	ns
ketamine 66 µg/mL	+0.0230	0.4464	0.052	0.959	ns

residual standard error = 3.156 (DF = 495)
multiple r-squared = 0.7, adjusted r-squared = 0.6975
F-statistic = 288.7 (DF=4, 495), p-value: < 2.2e-16

2.7.Experiment 6 (Fig.4B, Fig.S5)
brain weight (Fig.4Ba):
*fit_exp_6_abs_w_brain <- lm (w_brain ~ sex * drug, data = dataset_exp_6_brain_weight)*
summary (fit_exp_6_abs_w_brain)
Coefficients:

drug/sex	estimate	std. error	t-value	Pr(>|t|)	signif. code
(intercept)	+1.00174	0.01520	65.887	< 2e-16	***
sex	+0.03101	0.02135	1.453	0.148404	ns
VPA 5.82mg	−0.08410	0.02426	−3.467	0.000683	***
ketamine 0.20mg	−0.04889	0.02891	−1.691	0.092845	ns
tubocurarine 0.20mg	−0.03094	0.04246	−0.729	0.467397	ns
sex* VPA	+0.02942	0.03266	0.901	0.369059	ns
sex* ketamine	+0.01340	0.03939	0.340	0.734245	ns
sex* tubocurarine	+0.02419	0.06000	0.403	0.687336	ns

residual standard error = 0.08865 (DF = 153)
multiple r-squared = 0.1514, adjusted r-squared = 0.1126
F-statistic= 3.901 (Df = 7, 15), p-value = 0.0006117

body weight (Fig.S5)
*fit_exp_6_abs_w_body <- lm (w_body ~ sex * drug, data = dataset_exp_6_brain_weight)*
summary (fit_exp_6_abs_w_body)
Coefficients:

drug/sex	estimate	std. error	t-value	Pr(>|t|)	signif. code
(intercept)	+39.65882	0.54955	72.166	<2e-16	***
sex	+0.17832	0.87678	0.231	0.818	ns
VPA 5.82mg	−1.3451	0.02426	−1.534	0.127	ns
ketamine 0.20mg	−0.06652	0.02891	−0.064	0.949	ns
tubocurarine 0.20mg	+1.10118	1.53481	0.717	0.474	ns
sex* VPA	+0.85643	1.18040	0.726	0.469	ns
sex* ketamine	−1.36438	1.42373	−0.958	0.339	ns
sex* tubocurarine	−1.91832	2.16856	−0.885	0.378	ns

Residual standard error = 3.204 (DF = 153)
multiple r-squared = 0.03717, adjusted r-squared = -0.006877
F-statistic= 0.8439 (Df = 7, 153), p-value = 0.5527

total cell number (Fig.4Bb):

*fit_exp_6_cell_count <- lm(cell_number ~ sex * drug, data = dataset_exp_6_neuron_glia)*
summary (fit_exp_6_cell_count)

Coefficients:

drug/sex	estimate	std. error	t-value	Pr(>|t|)	signif. code
(intercept)	+32.806	3.128	10.488	6.97e-12	***
sex	+3.626	4.424	0.820	0.418	ns
VPA 5.82mg	−0.599	4.424	−0.135	0.893	ns
ketamine 0.20mg	−1.412	4.424	−0.319	0.752	ns
tubocurarine 0.20mg	+2.088	4.424	0.472	0.640	ns
sex* VPA	−2.719	6.256	−0.435	0.667	ns
sex* ketamine	−2.004	6.256	−0.320	0.751	ns
sex* tubocurarine	−5.436	6.256	−0.869	0.391	ns

residual standard error=6.994 (DF = 32)
multiple r-squared = 0.05307, adjusted r-squared = -0.1541
F-statistic= 0.2562 (Df = 7, 32), p-value = 0.9663

NeuN-positive cell ratio (Fig.4Bc)

*fit_exp_6_neuron_glia_ratio <- lm(neuron_ratio ~ sex * drug, data = dataset_exp_6_neuron_glia)*
summary (fit_exp_6_neuron_glia_ratio)

Coefficients:

drug/sex	estimate	std. error	t-value	Pr(>|t|)	signif. code
(intercept)	+0.522874	0.019104	27.370	<2e-16	***
sex	−0.073903	0.027017	0.632	0.5316	ns
VPA 5.82mg	−0.073903	0.027017	−2.735	0.0101	*
ketamine 0.20mg	+0.008096	0.027017	0.300	0.7664	ns
tubocurarine 0.20mg	−0.001942	0.027017	−0.072	0.9431	ns
sex* VPA	+0.025310	0.038208	0.662	0.5124	ns
sex* ketamine	−0.055518	0.038208	−1.453	0.1559	ns
sex* tubocurarine	−0.017455	0.038208	−0.457	0.6509	ns

residual standard error=0.04272 (DF = 32)
multiple r-squared = 0.3429, adjusted r-squared = 0.1991
F-statistic: 2.385 (Df=7, 32), p-value = 0.04411

2.8.Experiment 7 (Fig.4C)

nAChR a4/a7 ratio (log) (developmental changes, Fig.4Ca):

*fit_exp_7_chrna4_7_ratio <- lm(log(chrna4_7_ratio) ~ region * age, data = dataset_exp_7_development_2)*
summary (fit_exp_7_chrna4_7_ratio)

Coefficients:

region/age	estimate	std. error	t-value	Pr(>|t|)	signif. code
(intercept)	+0.6903	0.2409	2.865	0.006911	**
arcopallium	−1.2369	0.3407	−3.631	0.000872	***
tectum	−2.8964	0.3407	−8.501	3.94e-10	***
E18	+0.1690	0.3407	0.496	0.622867	ns
P1	−0.2252	0.3407	−0.661	0.512794	ns
arco*E18	+0.2131	0.4818	0.442	0.660903	ns
tectum*E18	−0.1297	0.4818	−0.269	0.789251	ns
arco*P1	+0.4578	0.4818	0.950	0.348341	ns
tectum*P1	+0.8696	0.4818	1.805	0.079460	ns

residual standard error = 0.5387 (DF = 36)
multiple r-squared = 0.8421, adjusted r-squared = 0.807
F-statistic: 23.99 (Df = 8, 36), p-value = 3.059e-12

slc12a2/a5 ratio (log) (developmental changes, Fig.4Cb):

*fit_exp_7_slc12a2_5_ratio <- lm(log(slc12a2_5_ratio) ~ region * age, data = dataset_exp_7_development_2)*
summary (fit_exp_7_slc12a2_5_ratio)

Coefficients:

region/age	estimate	std. error	t-value	Pr(>|t|)	signif. code
(intercept)	+0.09327	0.11978	0.779	0.441238	ns
arcopallium	−0.42871	0.16939	−2.531	0.015889	*
tectum	−0.82536	0.16939	−4.873	2.22e-05	***
E18	−0.71498	0.16939	−4.221	0.000157	***
P1	−1.63502	0.16939	−9.652	1.59e-11	***
arco*E18	−0.06802	0.23956	−0.284	0.778078	ns
tectum*E18	+0.20294	0.23956	0.847	0.402501	ns
arco*P1	+0.49020	0.23956	2.046	0.048086	*
tectum*P1	+1.08314	0.23956	4.521	6.42e-05	***

residual standard error = 0.2678 (DF = 36)
multiple r-squared = 0.8271, adjusted r-squared = 0.7886
F-statistic = 21.52 (DF= 8, 36), p-value = 1.489e-11

rbfox/GAPDH ratio (log) (developmental changes, Fig.4Cc):

*fit_exp_7_rbfox3 <- lm(log(rbfox3) ~ region * age, data = dataset_exp_7_development_2)*
summary (fit_exp_7_rbfox3)

Coefficients:

region/age	estimate	std. error	t-value	Pr(>|t|)	signif. code
(intercept)	−3.88036	0.19936	-19.464	< 2e-16	***
arcopallium	−0.02821	0.28194	−0.100	0.9208	ns
tectum	+0.48894	0.28194	1.734	0.0914	ns
E18	+0.60790	0.28194	2.156	0.0378	*
P1	+1.41950	0.28194	5.035	1.35e-05	***
arco*E18	−0.13882	0.39872	−0.348	0.7297	ns
tectum*E18	−0.26089	0.39872	−0.654	0.5171	ns
arco*P1	−0.88824	0.39872	−2.228	0.0322	*
tectum*P1	−0.70680	0.39872	−1.773	0.0847	ns

residual standard error = 0.4458 (DF = 36)
multiple r-squared = 0.5692, adjusted r-squared = 0.4735
F-statistic = 5.946 (DF = 8, 36), p-value = 7.234e-05

slc12a2/a5 ratio (log) (effects of VPA, Fig.4Ce):
*fit_exp_7_slc12a2_5_ratio_vpa <- lm(log(slc12a2_5_ratio) ~ region * drug, data = dataset_exp_7_vpa_2)*
summary (fit_exp_7_slc12a2_5_ratio_vpa)
Coefficients:

region/age	estimate	std. error	t-value	Pr(>|t|)	signif. code
(intercept)	-0.10636	0.10758	-0.989	0.331	ns
arcopallium	-0.04474	0.15215	-0.294	0.771	ns
tectum	-0.15263	0.15215	-1.003	0.324	ns
VPA 5.82mg	0.05273	0.15215	0.347	0.731	ns
arcopallium* VPA 5.82mg	0.08139	0.21517	0.378	0.708	ns
tectum * VPA 5.82mg	0.40891	0.21517	1.900	0.067	ns

residual standard error = 0.2635 (DF = 30)
multiple r-squared = 0.2581, adjusted r-squared = 0.1345
F-statistic = 2.088 (DF= 5, 30), p-value = 0.09461

slc12a2/a5 ratio (log) (effects of tubocurarine, Fig.4Cf):
*fit_exp_7_slc12a2_5_ratio_tubo <- lm(log(slc12a2_5_ratio) ~ region * drug, data = dataset_exp_7_tubo_2)*
summary (fit_exp_7_slc12a2_5_ratio_tubo)
Coefficients:

region/age	estimate	std. error	t-value	Pr(>|t|)	signif. code
(intercept)	−1.54175	0.11686	−13.193	1.71e-12	***
arcopallium	+0.06148	0.16526	0.372	0.713	ns
tectum	+0.25777	0.16526	1.560	0.132	ns
tubocurarine 0.20mg	+ 0.28104	0.16526	1.701	0.102	ns
arcopallium* tubocurarine 0.20mg	−0.21275	0.23372	−0.910	0.372	ns

tectum* tubocurarine 0.20mg	−0.24138	0.23372	−1.033	0.312	ns

residual standard error = 0.2613 (DF = 24)
multiple r-squared = 0.1934, adjusted r-squared = 0.0253
F-statistic = 1.151 (DF= 5, 24), p-value = 0.3617

2.9.Experiment 8 (Fig.5)

ballistography index explained by drug (Fig.5A):

fit_exp_1_ballistography_selected_bumeta_vu <- lm(ratio ~ label, data = dataset_exp_1_ballistography_bume_vu)
summary(fit_exp_1_ballistography_selected_bumeta_vu)

Coefficients:

drug	estimate	std. error	t-value	Pr(>|t|)	signif. code
(intercept)	1.18063	0.08848	13.343	2.11e-13	***
bumetanide (0.02mg)	-0.21975	0.14674	-1.498	0.146	ns
VU0463271 (0.2mg)	0.03569	0.14674	0.243	0.810	ns

residual standard error = 0.3311 (DF = 27)
multiple r-squared = 0.09874 , adjusted r-squared = 0.03198
F-statistic = 1.479 (DF = 2, 27), p-value = 0.2457

BM score explained by drug (Fig.5Ba):

fit_exp_8_bm <- lm (bm ~ label, data = dataset_exp_2_bm_imprint_ctrl_vpa_tubo_keta_bume_all)
summary (fit_exp_8_bm)

Coefficients:

drug	estimate	std. error	t-value	Pr(>|t|)	signif. code
(intercept)	136.31	16.62	8.200	4.74e-14	***
E14 VPA 5.82mg	26.09	60.63	0.430	0.66745	ns
E14 VPA 5.82mg + P1 bumetanide 0.02mg	-53.71	60.63	-0.886	0.37687	ns
E14 ketamine 0.2mg	-146.81	60.63	-2.422	0.01646	*
E14 ketamine 0.2mg + P1 bumetanide 0.02mg	-92.85	58.02	-1.600	0.11130	ns
E14 tubocurarine 0.2mg	-162.51	60.63	-2.629	0.00941	**
E14 tubocurarine 0.2mg + P1 bumetanide 0.02mg	-84.18	60.63	-1.227	0.22149	ns

residual standard error = 184.4 (DF = 177)
multiple r-squared = 0.07944, adjusted r-squared = 0.04824
F-statistic = 2.546 (DF = 6, 177), p-value = 0.02174

imprinting score explained by drug (Fig.5Bb):

fit_exp_8_imprint <- lm (imprint ~ label, data = dataset_exp_2_bm_imprint_ctrl_vpa_tubo_keta_bume_all)summary

(fit_exp_8_imprint)
Coefficients:

drug	estimate	std. error	t-value	Pr(>|t|)	signif. code
(intercept)	419.52	19.49	21.523	< 2e-16	***
E14 VPA 5.82mg	-316.22	71.08	-4.449	1.52e-05	***
E14 VPA 5.82mg + P1 bumetanide 0.02mg	84.68	71.08	1.191	0.2351	ns
E14 ketamine 0.2mg	-118.62	71.08	-1.669	0.0969	ns
E14 ketamine 0.2mg + P1 bumetanide 0.02mg	-26.07	68.03	-0.383	0.7021	ns
E14 tubocurarine 0.2mg	47.08	71.08	0.662	0.5086	ns
E14 tubocurarine 0.2mg + P1 bumetanide 0.02mg	-8.52	71.08	-0.076	0.9393	ns

residual standard error = 216.2 (DF = 177)
multiple r-squared = 0.1249, adjusted r-squared = 0.09523
F-statistic = 4.21 (DF = 6, 177), p-value = 0.0005501

References

- Herculano-Houzel S, Lent R. (2005). Isotropic fractionator: a simple, rapid method for the quantification of total cell and neuron numbers in the brain. *Journal of Neuroscience* 25: 2518-2521 (doi: 10.1523/JNEUROSCI.4526-04.2005)
- Miura M, Matsushima T. (2012). Preference for biological motion in domestic chicks: sex-dependent effect of early visual experience. *Animal Cognition* 15: 871-879. (https://doi.org/10.1007/s10071-012-0514-x)
- Miura M, Matsushima T. (2016). Biological motion facilitates imprinting. *Animal Behaviour* 116: 171-180 (https://doi.org/10.1016/j.anbehav.2016.03.025)
- Miura M, Aoki N, Yamaguchi S, Homma K-J, Matsushima T. (2018). Thyroid hormone sensitizes the imprinting-associated induction of biological motion preference in domestic chicks. *Frontiers in Physiology (Avian Physiology)* 9:1740 (https://doi.org/10.3389/fphys.2018.01740)
- Miura M, Nishi D, Matsushima T. (2020). Combined predisposed preferences for colour and biological motion make robust development of social attachment through imprinting. *Animal Cognition* 23: 169-188 (doi https://doi.org/10.1007/s10071-019-01327-5)
- Suzuki Y, Musashi H, Tazawa H. (1989). Noninvasive heart rate monitoring system for avian embryos based on the ballistocardiogram. *Medical and Biological Engineering & Computing* 27: 399-404
- Taguchi G, Rajesh J. (2000). New trends in multivariate diagnosis. *Indian Journal of Statistics* 62: 233-238
- Takemura Y, Yamaguchi S, Aoki N, Miura M, Homma KJ, Matsushima T. (2018). Gene expression of Dio2 (thyroid hormone converting enzyme) in telencephalon is linked with predisposed biological motion preference in domestic chicks. *Behavioural Brain Research* 349: 25-30 (https://doi.org/10.1016/j.bbr.2018.04.039)

graphical summary

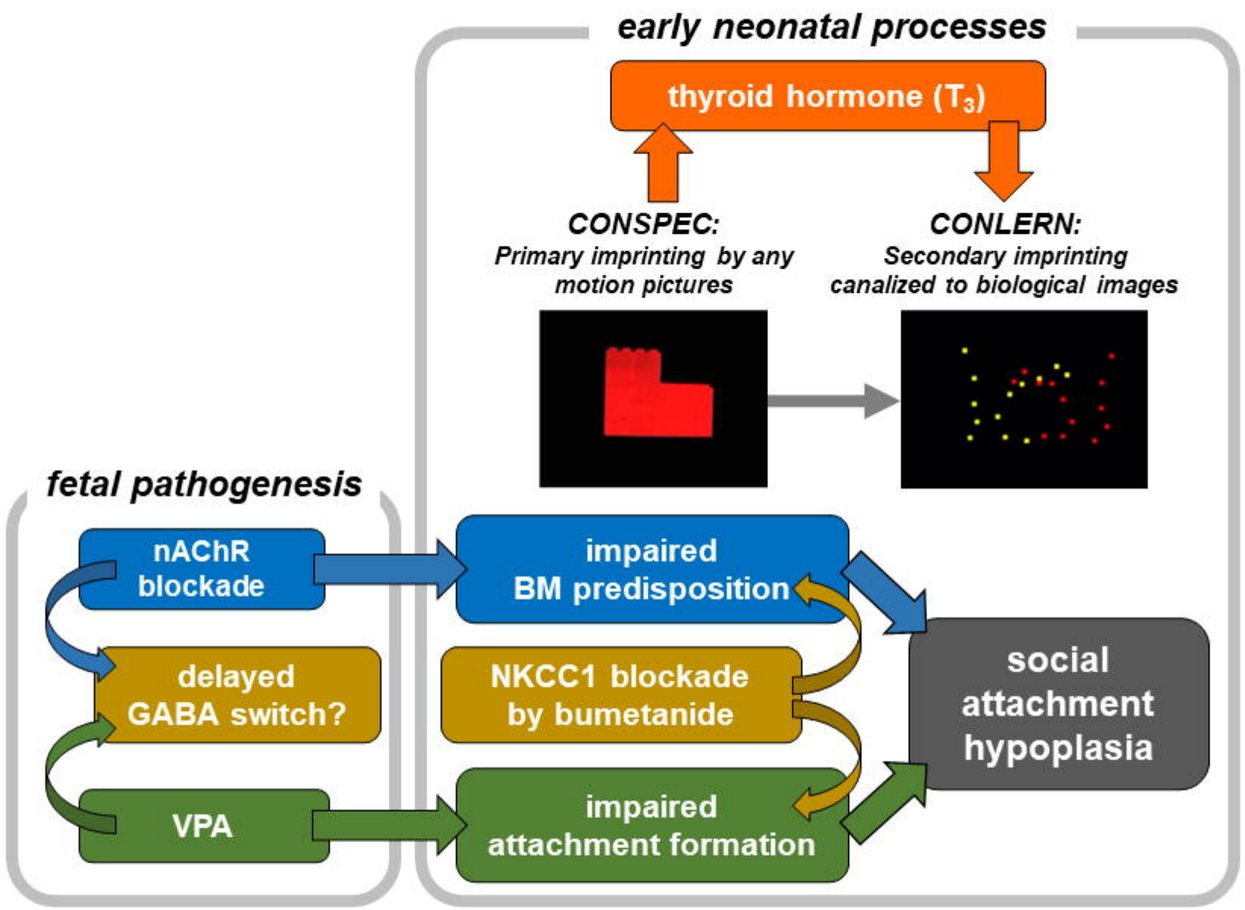

- Imprinting of artifact **canalizes** predisposed preference to **biological motion** (BM).
- Fetal **VPA** injection impairs imprinting and spares BM preference in hatchlings.
- Blockade of **nAChR** by ketamine or imidacloprid spares imprinting and impairs BM.
- Underlying molecular actions are **dissociated** between the two sets of chemicals.
- However, VPA and nAChR blockade impaired the **imprinting of biological images**.
- Both impairments are rescued by postnatal **bumetanide**.

figure_1

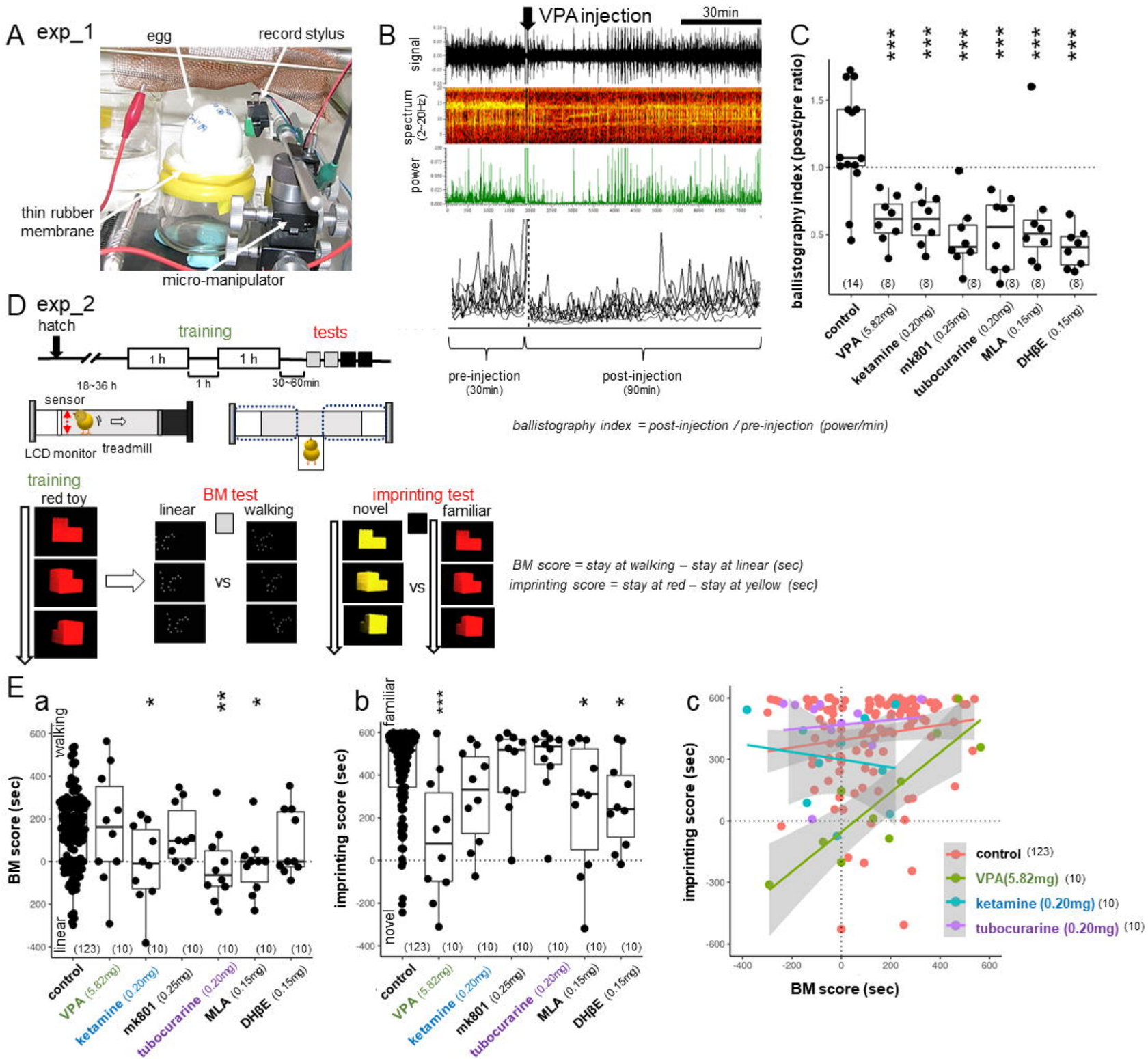
A exp_1
egg
record stylus
thin rubber membrane
micro-manipulator
B
VPA injection
30min
signal
spectrum (2~20Hz)
power
pre-injection (30min)
post-injection (90min)
C
ballistography index (post/pre ratio)
control
VPA (5.82mg)
ketamine (0.20mg)
mk801 (0.25mg)
tubocurarine (0.20mg)
MLA (0.15mg)
DHβE (0.15mg)
ballistography index = post-injection / pre-injection (power/min)
D exp_2
hatch
training
tests
1 h
1 h
18~36 h
1 h
30~60min
sensor
LCD monitor
treadmill
training
red toy
BM test
linear
walking
vs
imprinting test
novel
familiar
vs
BM score = stay at walking – stay at linear (sec)
imprinting score = stay at red – stay at yellow (sec)
E
a
BM score (sec)
walking
linear
b
imprinting score (sec)
familiar
novel
c
imprinting score (sec)
BM score (sec)
control (123)
VPA(5.82mg) (10)
ketamine (0.20mg) (10)
tubocurarine (0.20mg) (10)

figure_2

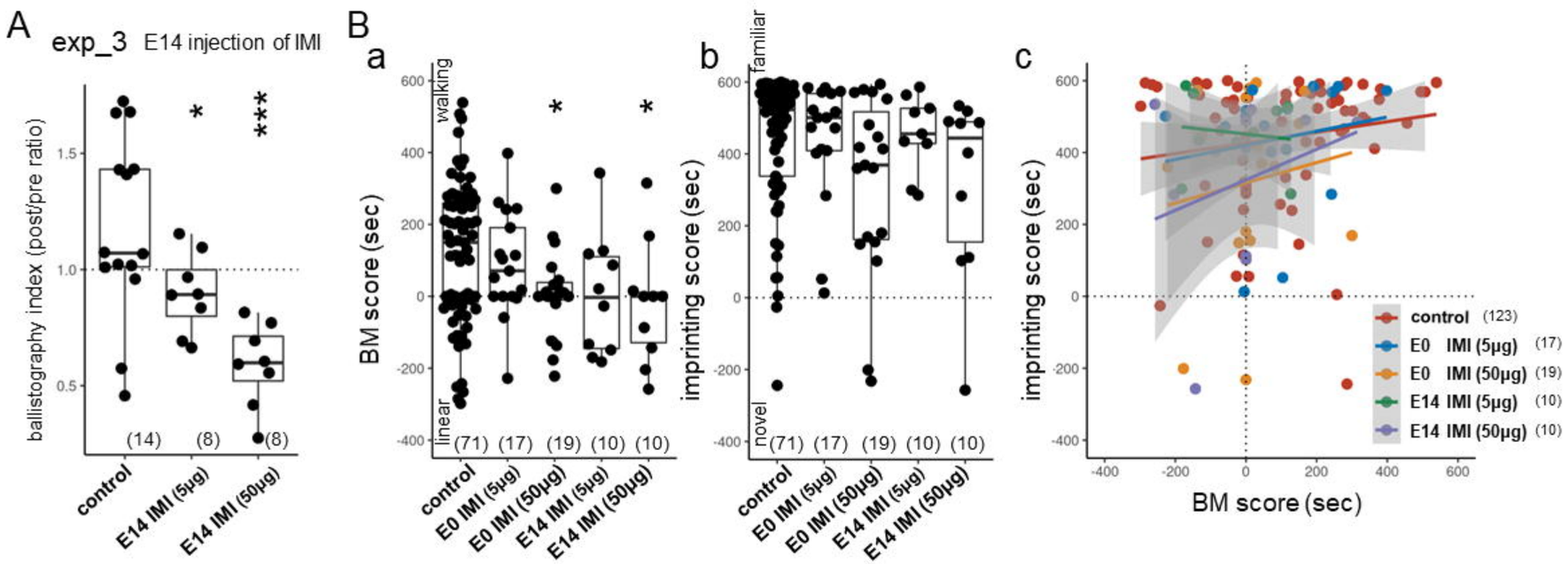
A
exp_3 E14 injection of IMI
ballistography index (post/pre ratio)
1.5
1.0
0.5
*
***
(14)
(8)
(8)
control
E14 IMI (5μg)
E14 IMI (50μg)
B
a
walking
linear
BM score (sec)
600
400
200
0
-200
-400
*
*
(71) (17) (19) (10) (10)
control
E0 IMI (5μg)
E0 IMI (50μg)
E14 IMI (5μg)
E14 IMI (50μg)
b
familiar
novel
imprinting score (sec)
(71) (17) (19) (10) (10)
c
imprinting score (sec)
BM score (sec)
-400
-200
0
200
400
600
control (123)
E0 IMI (5μg) (17)
E0 IMI (50μg) (19)
E14 IMI (5μg) (10)
E14 IMI (50μg) (10)

figure_3

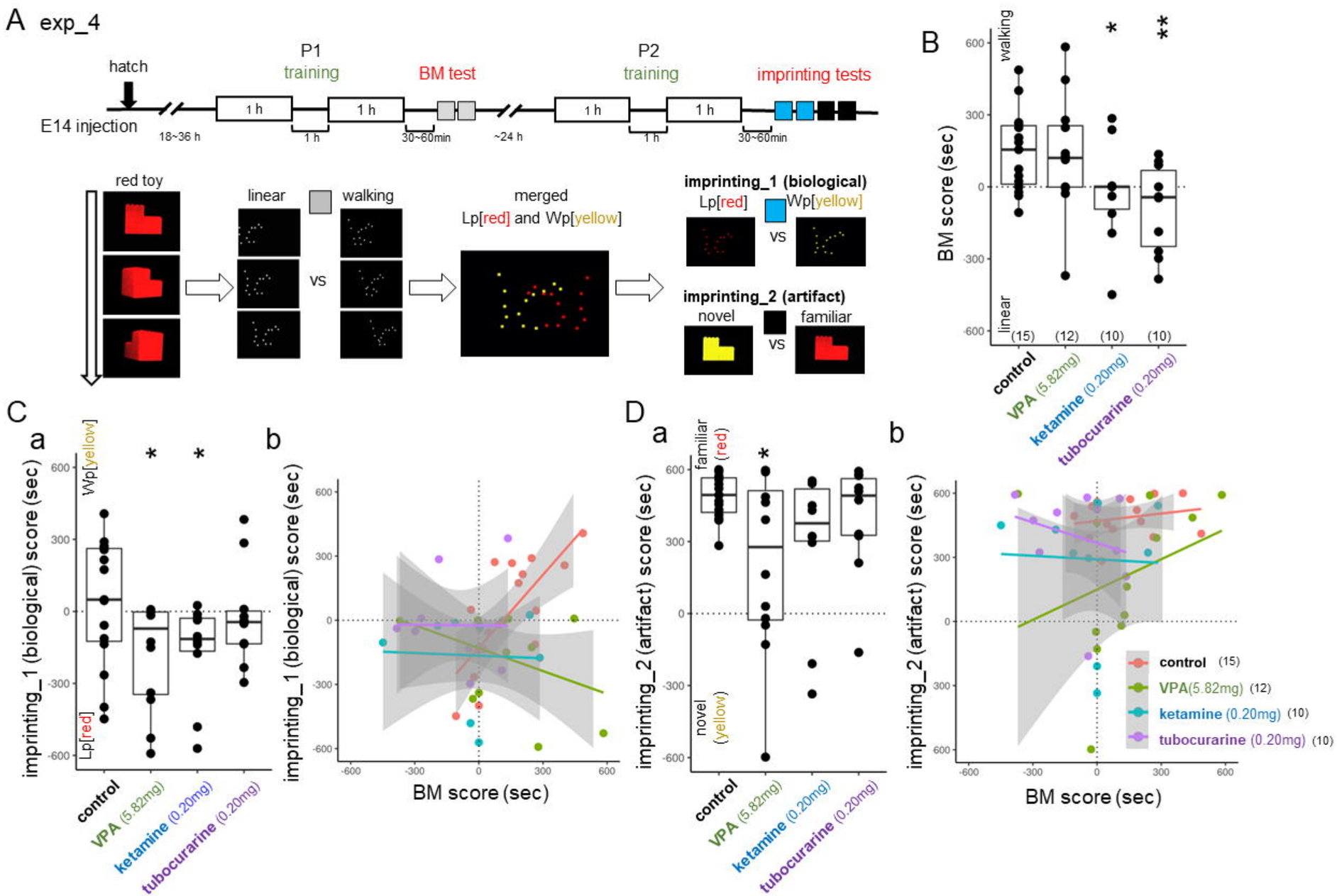
A exp_4
hatch
E14 injection
18~36 h
P1
training
1 h
1 h
BM test
30~60min
~24 h
P2
training
1 h
1 h
imprinting tests
30~60min
red toy
linear
walking
vs
merged
Lp[red] and Wp[yellow]
imprinting_1 (biological)
Lp[red]
Wp[yellow]
vs
imprinting_2 (artifact)
novel
familiar
vs
B
BM score (sec)
walking
linear
(15)
(12)
(10)
(10)
control
VPA (5.82mg)
ketamine (0.20mg)
tubocurarine (0.20mg)
C
a
imprinting_1 (biological) score (sec)
Wp[yellow]
Lp[red]
control
VPA (5.82mg)
ketamine (0.20mg)
tubocurarine (0.20mg)
b
imprinting_1 (biological) score (sec)
BM score (sec)
D
a
imprinting_2 (artifact) score (sec)
familiar (red)
novel (yellow)
control
VPA (5.82mg)
ketamine (0.20mg)
tubocurarine (0.20mg)
b
imprinting_2 (artifact) score (sec)
BM score (sec)
control (15)
VPA(5.82mg) (12)
ketamine (0.20mg) (10)
tubocurarine (0.20mg) (10)

figure_4

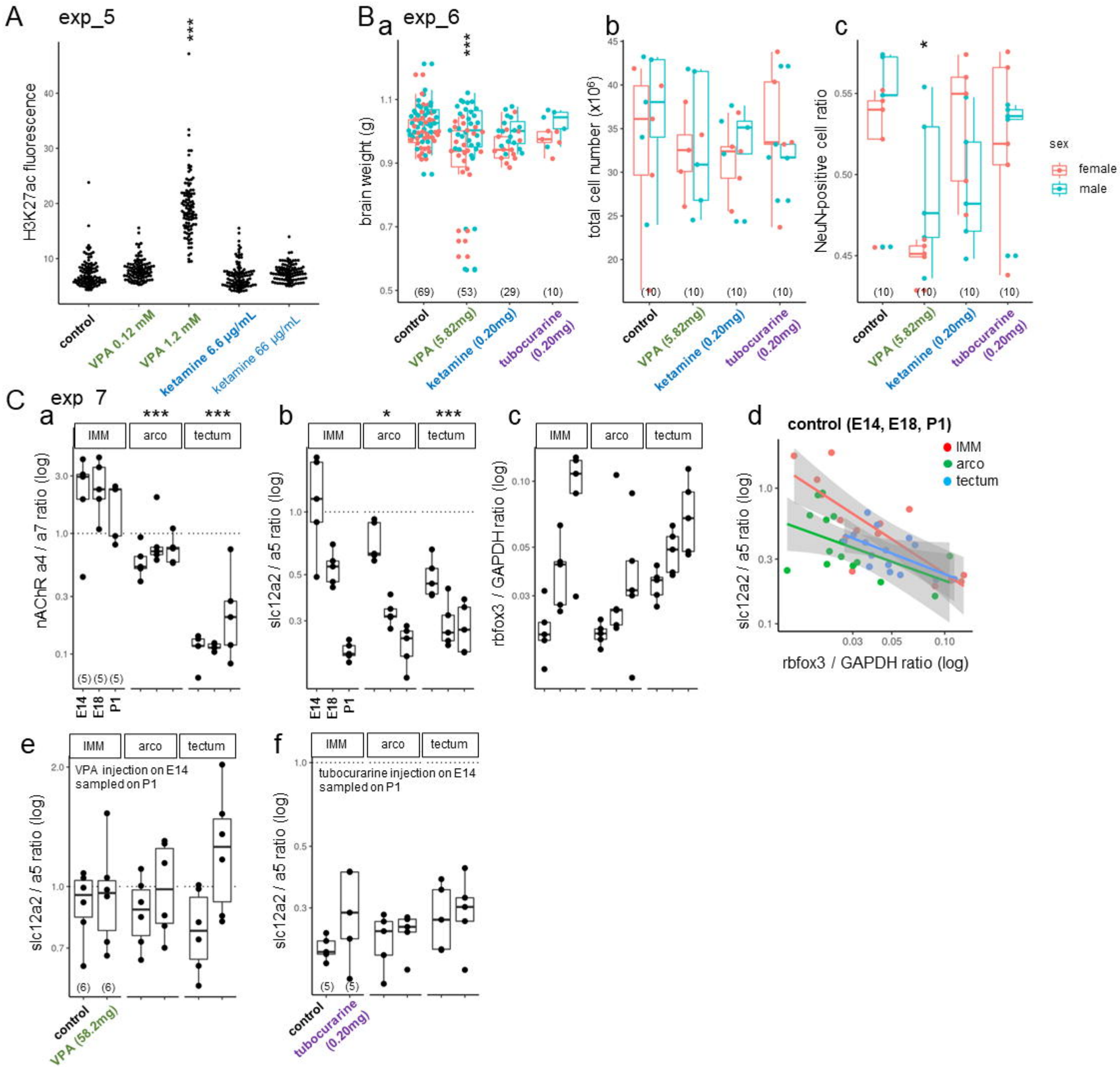
A
exp_5
H3K27ac fluorescence
control
VPA 0.12 mM
VPA 1.2 mM
ketamine 6.6 μg/mL
ketamine 66 μg/mL
B a
exp_6
brain weight (g)
(69) (53) (29) (10)
control
VPA (5.82mg)
ketamine (0.20mg)
tubocurarine (0.20mg)
b
total cell number (x10^6)
c
NeuN-positive cell ratio
sex
female
male
C a
exp 7
IMM
arco
tectum
nAChR a4 / a7 ratio (log)
E14
E18
P1
b
slc12a2 / a5 ratio (log)
c
rbfox3 / GAPDH ratio (log)
d
control (E14, E18, P1)
IMM
arco
tectum
slc12a2 / a5 ratio (log)
rbfox3 / GAPDH ratio (log)
e
VPA injection on E14
sampled on P1
slc12a2 / a5 ratio (log)
control
VPA (58.2mg)
f
tubocurarine injection on E14
sampled on P1
slc12a2 / a5 ratio (log)
control
tubocurarine (0.20mg)

figure_5

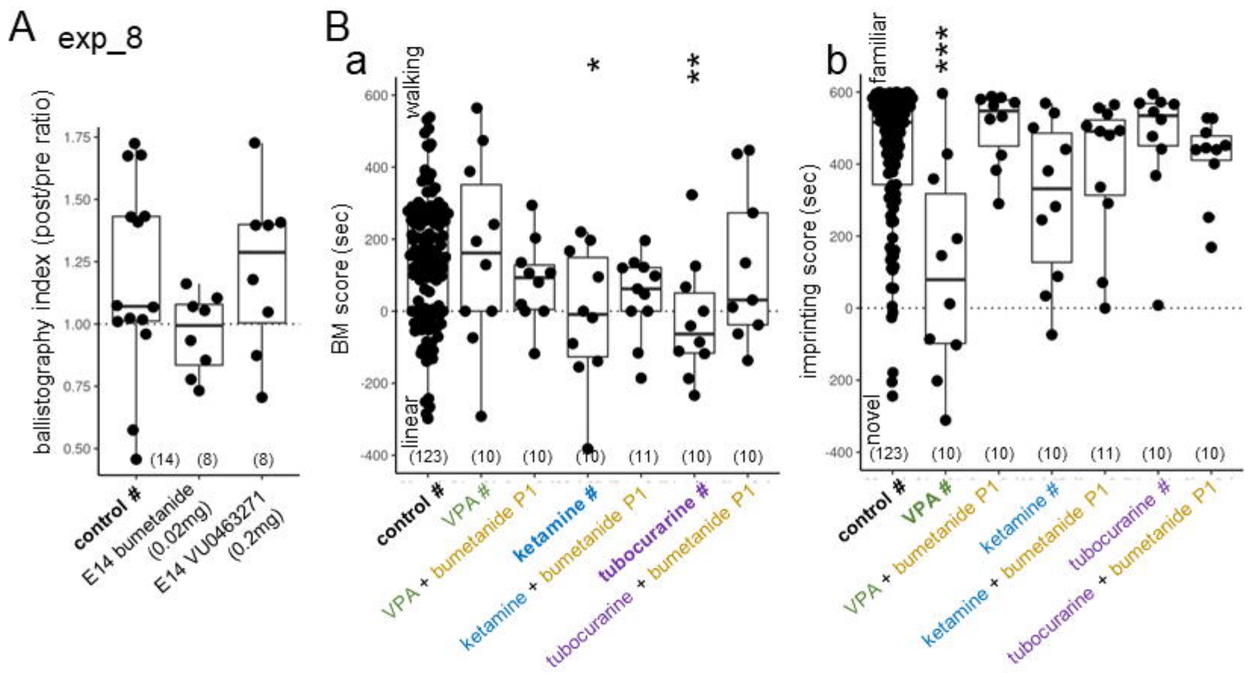
A
exp_8
ballistography index (post/pre ratio)
1.75
1.50
1.25
1.00
0.75
0.50
(14)
(8)
(8)
control #
E14 bumetanide (0.02mg)
E14 VU0463271 (0.2mg)
B
a
BM score (sec)
walking
linear
600
400
200
0
-200
-400
*
**
(123)
(10)
(10)
(10)
(11)
(10)
(10)
control #
VPA #
VPA + bumetanide P1
ketamine #
ketamine + bumetanide P1
tubocurarine #
tubocurarine + bumetanide P1
b
imprinting score (sec)
familiar
novel
***
(123)
(10)
(10)
(10)
(11)
(10)
(10)
control #
VPA #
VPA + bumetanide P1
ketamine #
ketamine + bumetanide P1
tubocurarine #
tubocurarine + bumetanide P1

figure_S1

A exp_0

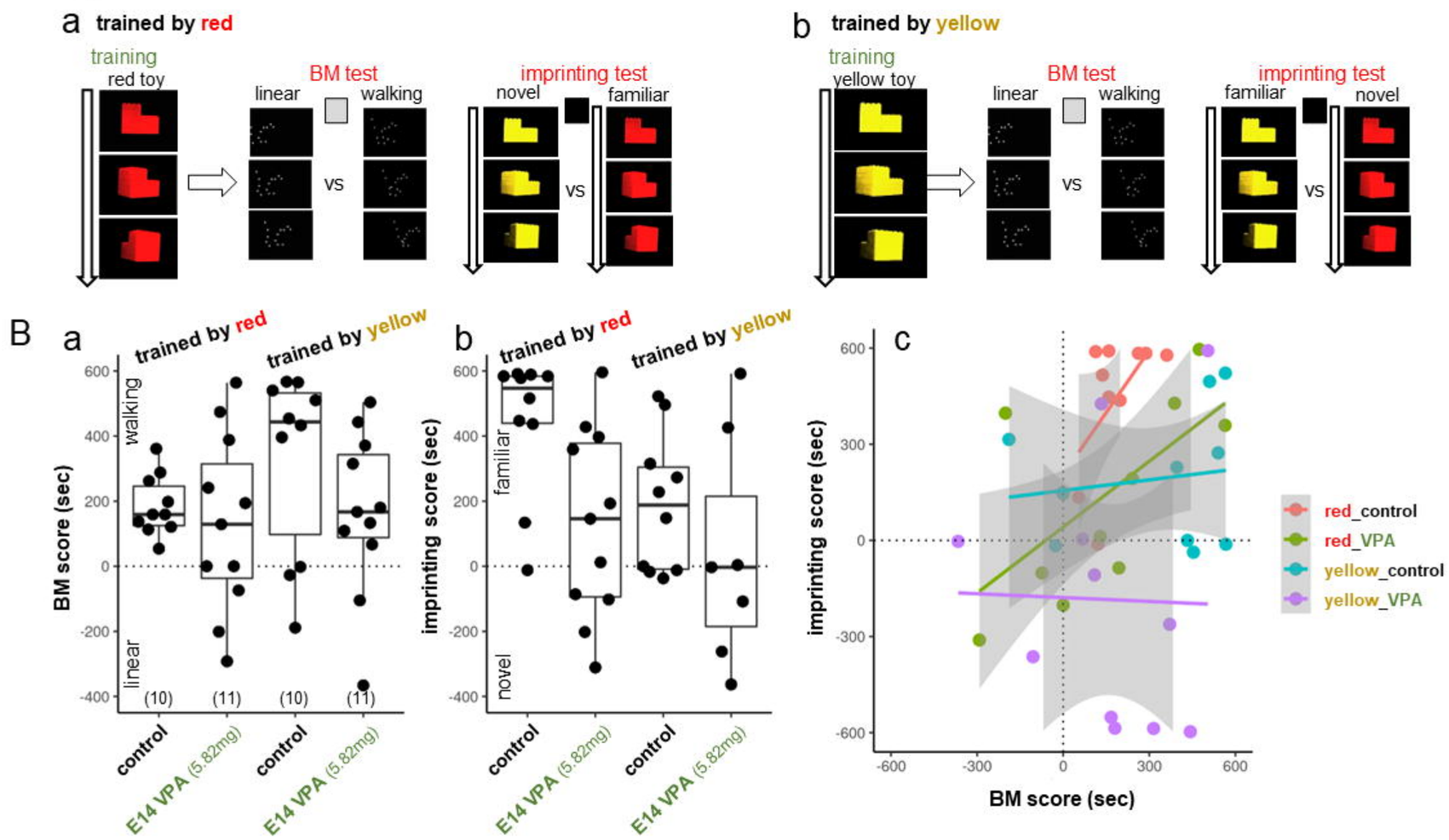

C

Analysis of Variance Table
Response: **bm**

	Df	Sum Sq	Mean Sq	F value	Pr(>F)
drug	1	121363	121363	2.1140	0.1542
colour	1	76288	76288	1.3289	0.2562
drug:colour	1	28105	28105	0.4896	0.4884
Residuals	38	2181492	57408		

Analysis of Variance Table
Response: **imprint**

	Df	Sum Sq	Mean Sq	F value	Pr(>F)
drug	1	1252323	1252323	14.0827	0.0005838 ***
colour	1	856572	856572	9.6324	0.0036004 **
drug:colour	1	10032	10032	0.1128	0.7388093
Residuals	38	3379199	88926		

figure_S2

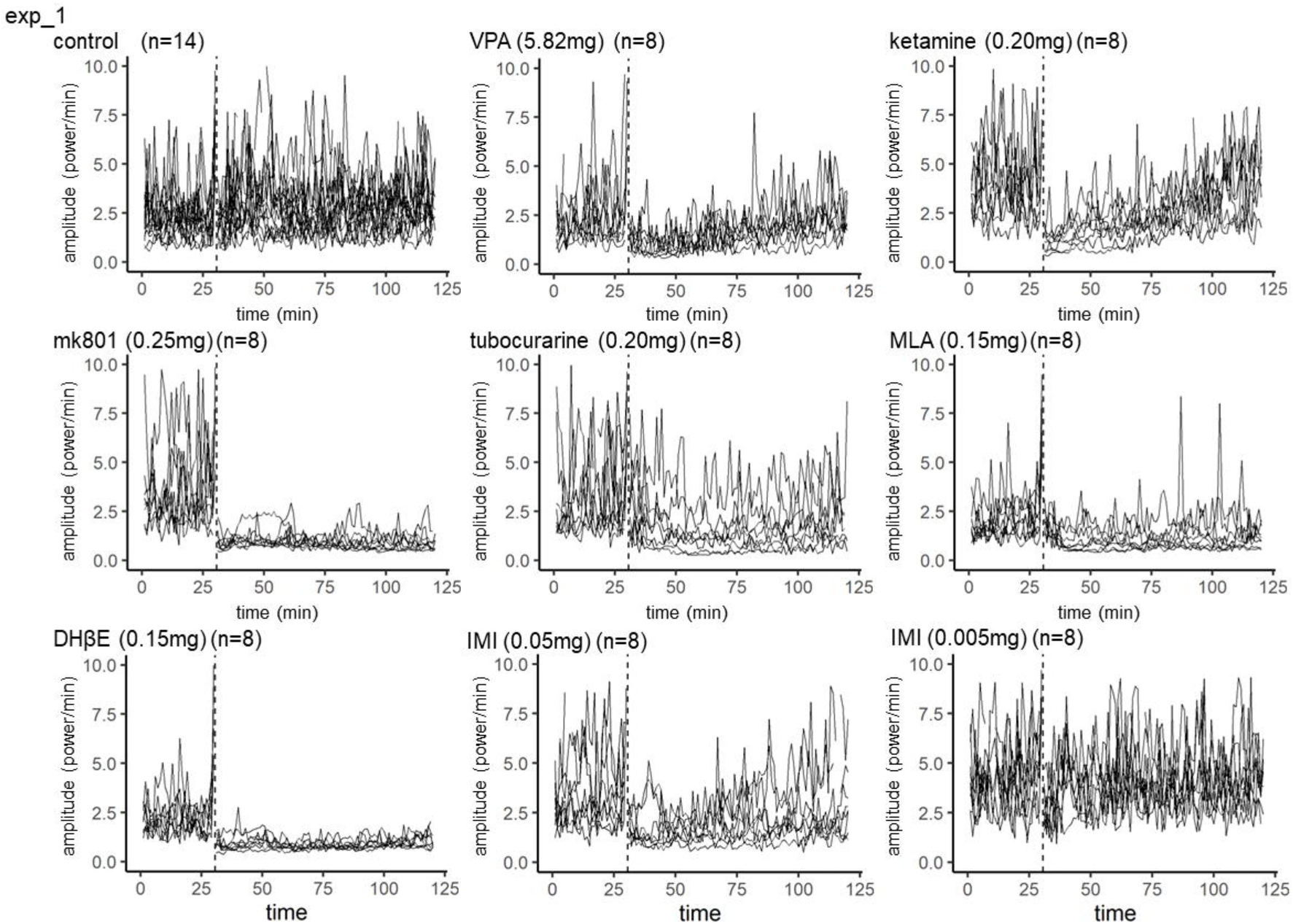
exp_1
control (n=14)
VPA (5.82mg) (n=8)
ketamine (0.20mg) (n=8)
mk801 (0.25mg) (n=8)
tubocurarine (0.20mg) (n=8)
MLA (0.15mg) (n=8)
DHβE (0.15mg) (n=8)
IMI (0.05mg) (n=8)
IMI (0.005mg) (n=8)
amplitude (power/min)
time (min)
time
0.0
2.5
5.0
7.5
10.0
0
25
50
75
100
125

figure_S3

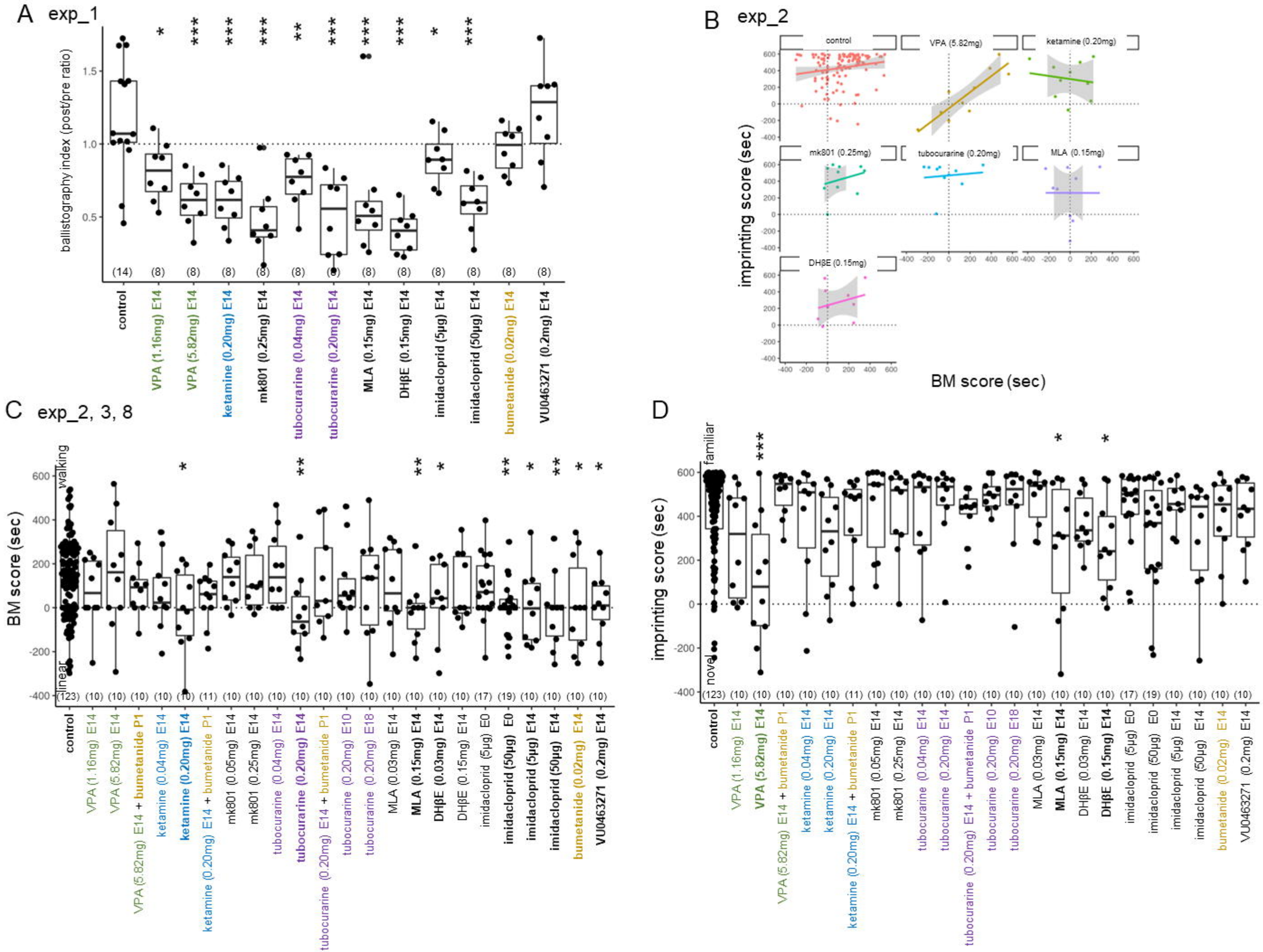
A exp_1
ballistography index (post/pre ratio)
control
VPA (1.16mg) E14
VPA (5.82mg) E14
ketamine (0.20mg) E14
mk801 (0.25mg) E14
tubocurarine (0.04mg) E14
tubocurarine (0.20mg) E14
MLA (0.15mg) E14
DHβE (0.15mg) E14
imidacloprid (5μg) E14
imidacloprid (50μg) E14
bumetanide (0.02mg) E14
VU0463271 (0.2mg) E14
B exp_2
imprinting score (sec)
BM score (sec)
control
VPA (5.82mg)
ketamine (0.20mg)
mk801 (0.25mg)
tubocurarine (0.20mg)
MLA (0.15mg)
DHβE (0.15mg)
C exp_2, 3, 8
BM score (sec)
walking
linear
D
imprinting score (sec)
familiar
novel

figure_S4

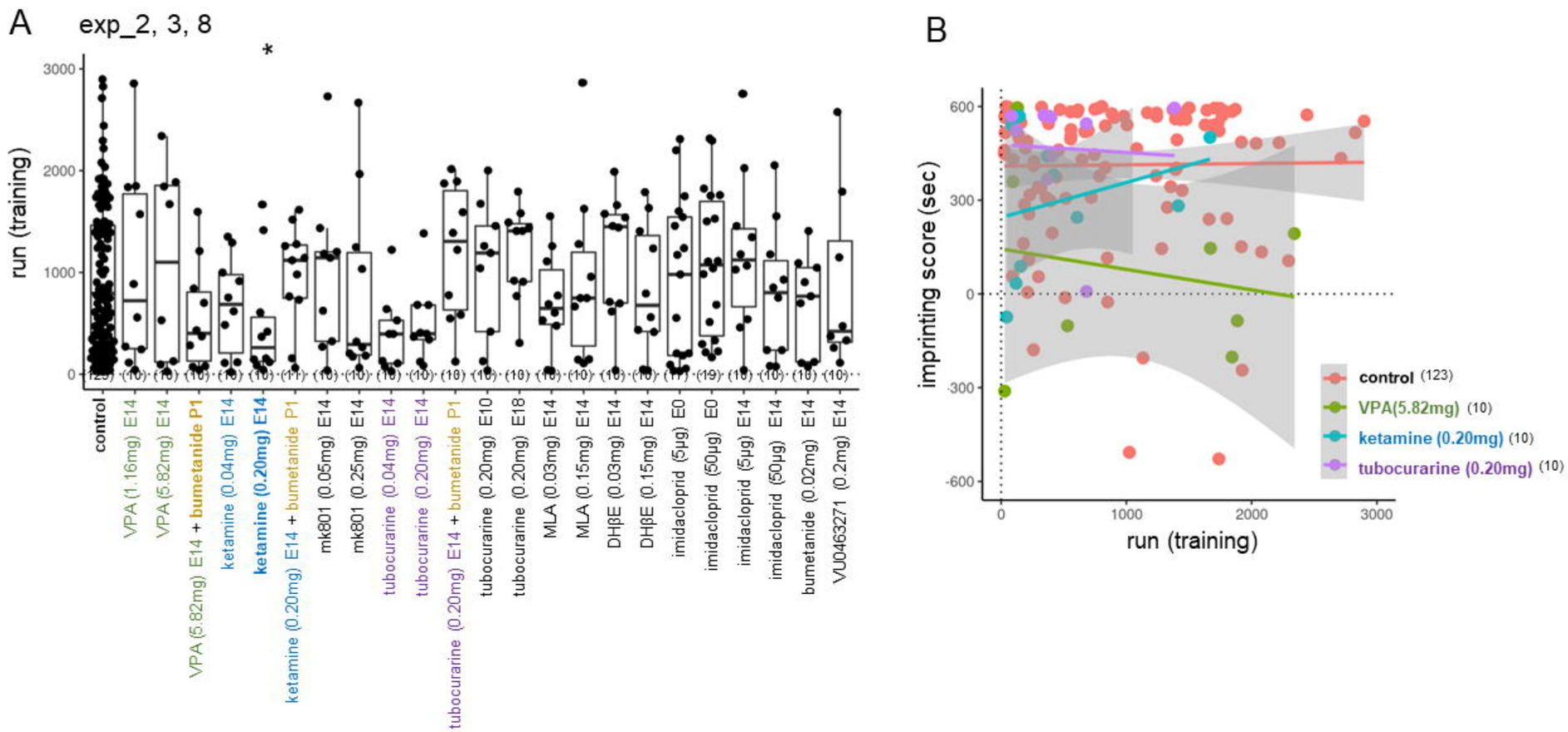
A
exp_2, 3, 8
*
run (training)
3000
2000
1000
0
control (123)
VPA (1.16mg) E14 (10)
VPA (5.82mg) E14 (10)
VPA (5.82mg) E14 + bumetanide P1 (10)
ketamine (0.04mg) E14 (10)
ketamine (0.20mg) E14 (10)
ketamine (0.20mg) E14 + bumetanide P1 (11)
mk801 (0.05mg) E14 (10)
mk801 (0.25mg) E14 (10)
tubocurarine (0.04mg) E14 (10)
tubocurarine (0.20mg) E14 (10)
tubocurarine (0.20mg) E14 + bumetanide P1 (10)
tubocurarine (0.20mg) E10 (10)
tubocurarine (0.20mg) E18 (10)
MLA (0.03mg) E14 (10)
MLA (0.15mg) E14 (10)
DHβE (0.03mg) E14 (10)
DHβE (0.15mg) E14 (10)
imidacloprid (5μg) E0 (11)
imidacloprid (50μg) E0 (19)
imidacloprid (5μg) E14 (10)
imidacloprid (50μg) E14 (10)
bumetanide (0.02mg) E14 (10)
VU0463271 (0.2mg) E14 (10)
B
imprinting score (sec)
600
300
0
-300
-600
0
1000
2000
3000
run (training)
control (123)
VPA(5.82mg) (10)
ketamine (0.20mg) (10)
tubocurarine (0.20mg) (10)

figure_S5

A

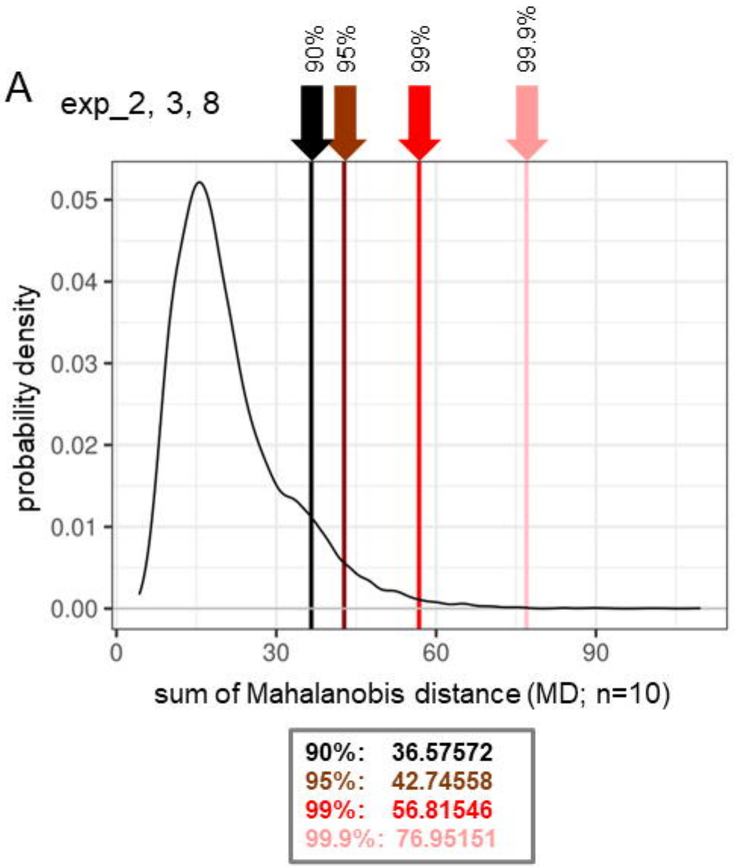

B

group (drug)	n	MD distance #	siginif. code
VPA 5.82mg	10	52.37958	*
VPA + bumetanide (P1)	10	8.294349	ns
ketamine 0.20mg	10	28.35494	ns
ketamine 0.20mg + bumetanide (P1)	11	14.25449	ns
mk801 0.25mg	10	11.97952	ns
tubocurarine 0.20mg	10	22.61997	ns
tubocurarine + bumetanide (P1)	10	23.78085	ns
MLA 0.15mg	10	33.41734	ns
DHβE 0.15mg	10	19.22331	ns
E0 IMI 0.005mg#	17	12.70195	ns
E0 IMI 0.05mg#	19	22.40369	ns
E14 IMI 0.005mg	10	28.34648	ns
E14 IMI 0.05mg	10	36.14058	ns

MD distance is normalized by the factor of 10/n.

figure_S6

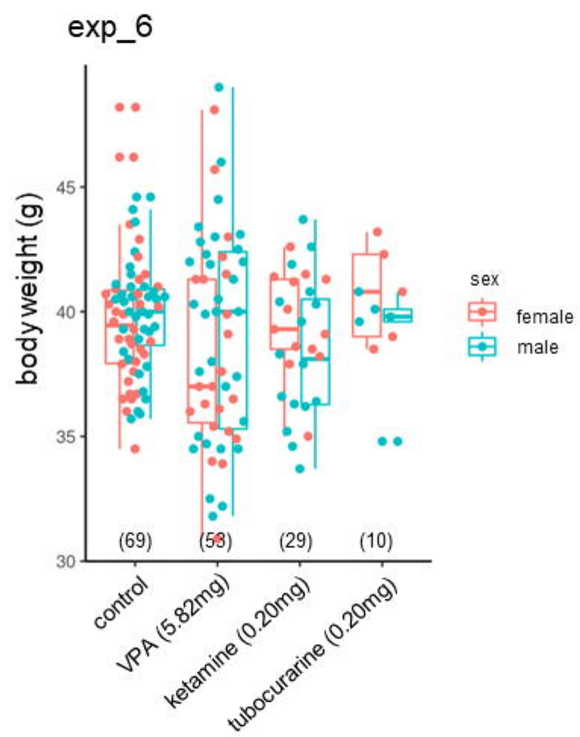
exp_6
body weight (g)
45
40
35
30
(69)
(58)
(29)
(10)
control
VPA (5.82mg)
ketamine (0.20mg)
tubocurarine (0.20mg)
sex
female
male

figure_S7

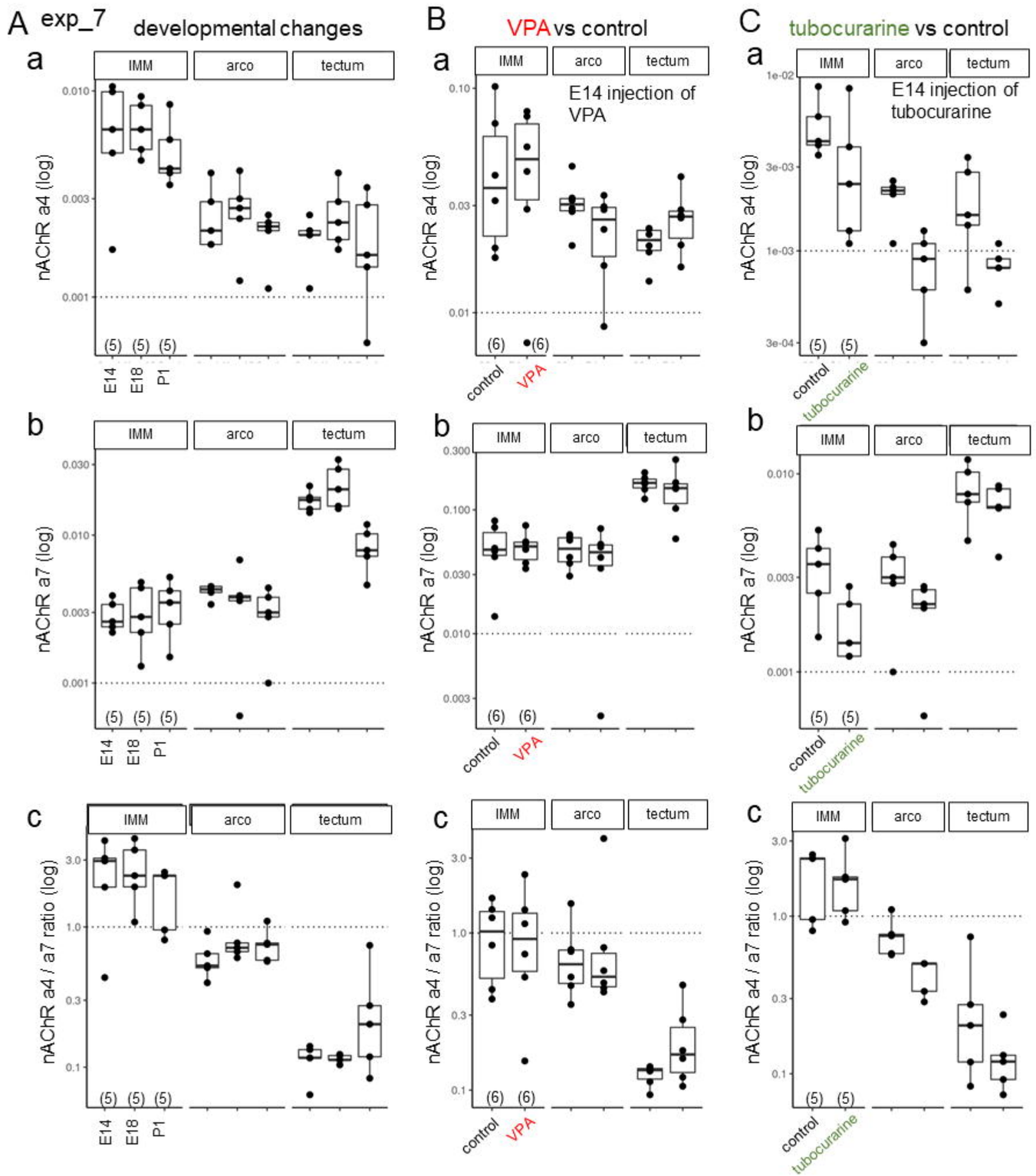
A exp_7
developmental changes
B
VPA vs control
C
tubocurarine vs control
a
b
c
IMM
arco
tectum
E14 injection of VPA
E14 injection of tubocurarine
nAChR a4 (log)
nAChR a7 (log)
nAChR a4 / a7 ratio (log)
E14
E18
P1
control
VPA
tubocurarine

figure_S8

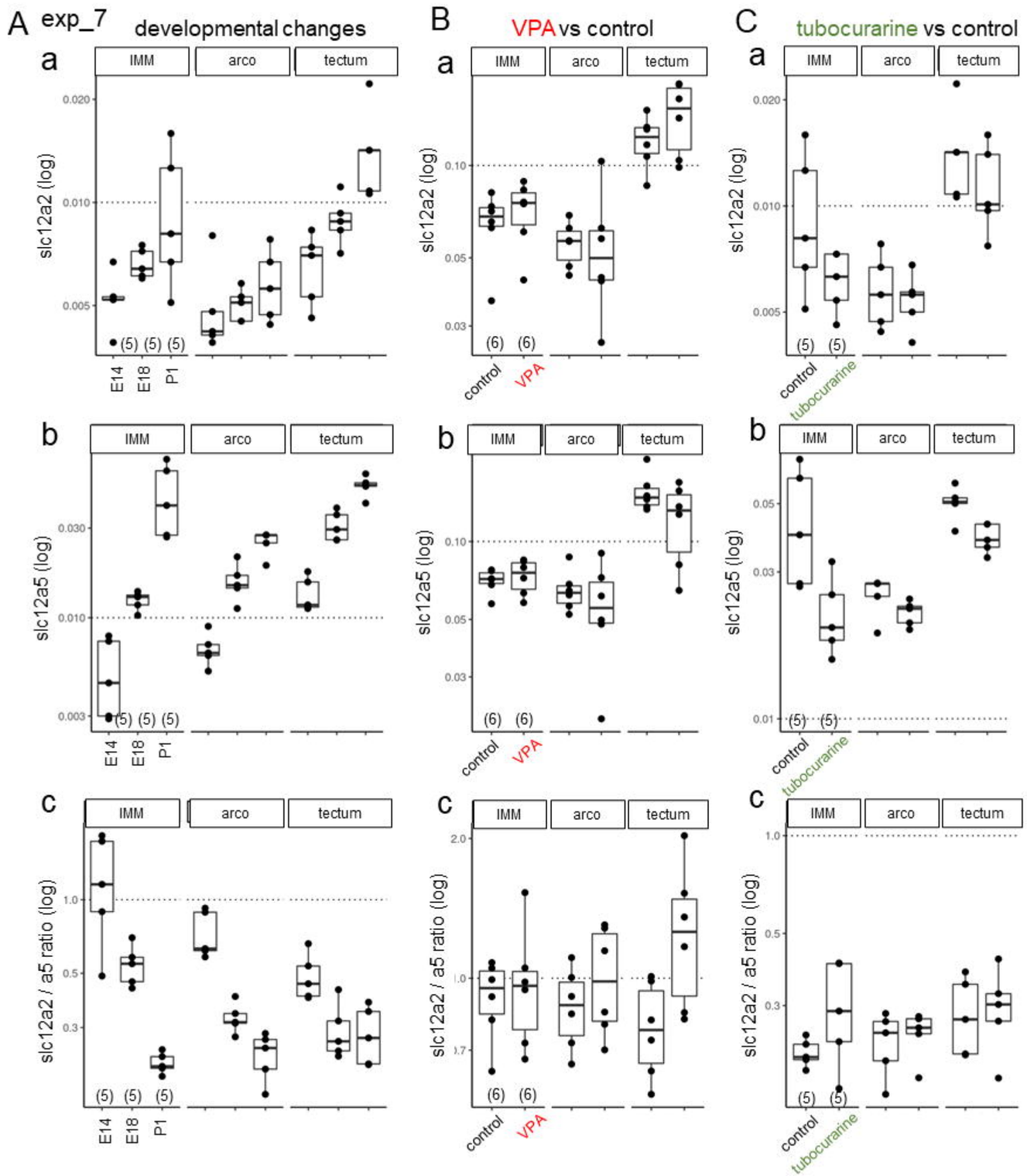
A exp_7
developmental changes
B
VPA vs control
C
tubocurarine vs control
a
b
c
IMM
arco
tectum
slc12a2 (log)
slc12a5 (log)
slc12a2 / a5 ratio (log)
(5) (5) (5)
(6) (6)
(5) (5)
E14
E18
P1
control
VPA
tubocurarine

figure_S9

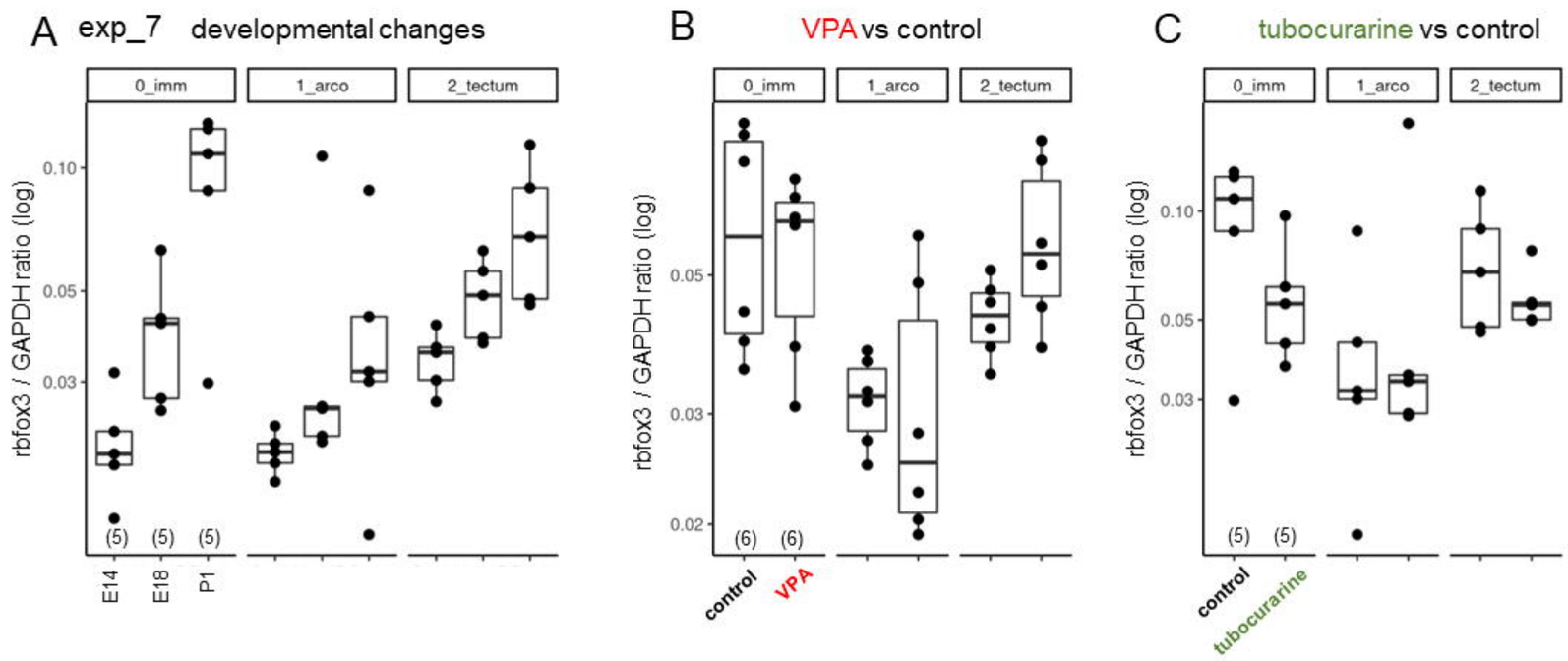
A exp_7 developmental changes
0_imm
1_arco
2_tectum
rbfox3 / GAPDH ratio (log)
0.10
0.05
0.03
(5)
(5)
(5)
E14
E18
P1
B VPA vs control
0_imm
1_arco
2_tectum
rbfox3 / GAPDH ratio (log)
0.05
0.03
0.02
(6)
(6)
control
VPA
C tubocurarine vs control
0_imm
1_arco
2_tectum
rbfox3 / GAPDH ratio (log)
0.10
0.05
0.03
(5)
(5)
control
tubocurarine